SPECIAL REPORT 96-12

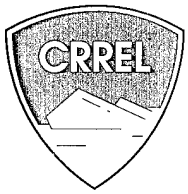

PCC Airfield Pavement Response During Thaw-Weakening Periods

A Field Study

Vincent C. Janoo and Richard L. Berg

May 1996

Abstract

This investigation is part of CRREL's on-going characterization of pavement performance in seasonal frost areas. As part of the research, CRREL conducted several field studies for the Federal Aviation Administration (FAA) on the response of airport pavements during thaw-weakening periods at three civil airports in Wisconsin, where the design freezing index in the area was around 900 to 1100°C-days and frost penetration ranged between 1250 to 2000 mm. This study focused on the performance of Portland Cement Concrete (PCC) pavements during the spring thaw-weakening period. The sites were instrumented with subsurface thermocouples and Falling Weight Deflectometer (FWD) tests were conducted during the spring thaw period at the center of the slab and across the joints. An analysis of the FWD data and backcalculation of the layer moduli using ILLIBACK and WESDEF was conducted. Unique relationships between the FWD deflections and the subgrade modulus and coefficient of subgrade reaction were obtained. Additional relationships were developed using the FWD deflections, PCC thickness and the horizontal tensile stress at the bottom of the PCC layer. A relationship between load transfer across joints and FWD deflections was also developed. On the basis of the relationships obtained in this study, a methodology for evaluating PCC pavements during spring thaw was developed. However, this methodology needs to be verified for other subgrade types and areas with other design freezing indices.

For conversion of SI units to non-SI units of measurement consult *Standard Practice for Use of the International System of Units (SI)*, ASTM Standard E380-93, published by the American Society for Testing and Materials, 1916 Race St., Philadelphia, Pa. 19103.

Special Report 96-12

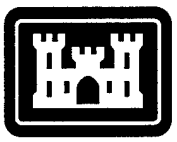

US Army Corps of Engineers
Cold Regions Research & Engineering Laboratory

PCC Airfield Pavement Response During Thaw-Weakening Periods

A Field Study

Vincent C. Janoo and Richard L. Berg

May 1996

Prepared for
FEDERAL AVIATION ADMINISTRATION
and
OFFICE OF THE CHIEF OF ENGINEERS

PREFACE

This report was prepared by Dr. Vincent C. Janoo and Dr. Richard L. Berg, Research Civil Engineers, Civil and Geotechnical Engineering Research Division, Research and Engineering Directorate, U.S. Army Cold Regions Research and Engineering Laboratory. Funding was provided by the Federal Aviation Administration and the Office of the Chief of Engineers. The OCE portion was funded through DA Project 4A762784 AT42, *Design, Construction and Operations Technology for Cold Regions*; Mission Area, *Base Support*; Work Unit BS/036, *Improved Pavement Design Criteria in Cold Regions*.

Technical review of the manuscript of this report was provided by Dr. Raymond Rollings (U.S. Army Engineer Waterways Experiment Station) and Michel Hovan (FAA). The authors express special thanks to L. Barna and F. Carver for assisting in the data reduction and for their patience, and to R. Guyer and C. Berini for gathering the data.

CONTENTS

ILLUSTRATIONS

Figure

Figure

TABLES

Table

PCC Airfield Pavement Response During Thaw-Weakening Periods
A Field Study

VINCENT C. JANOO AND RICHARD L. BERG

INTRODUCTION

In the spring of 1986, CRREL conducted a field study for the Federal Aviation Administration (FAA) on how airport pavements responded to frost action. The emphasis was on thaw weakening. The study was conducted at three regional airports in Wisconsin—Central Wisconsin Airport (CWA), Outagamie County Airport (OCA) and Wittman Field. The pavement surfaces at CWA and OCA were predominately Portland Cement Concrete (PCC), whereas at Wittman they were mostly Asphalt Concrete (AC). The results of a study on AC airfield pavement structures during thaw-weakening periods can be found in a previously published report (Janoo and Berg 1991). This report examines PCC airport pavements during thaw periods.

It is accepted that in the winter the load carrying capacity of pavements increases dramatically because of freezing of the pavement structure. This is more dramatic in AC pavements because of the stiffening of the asphalt at low temperatures. This increase is also seen in PCC pavements because of a similar stiffening of the base, subbase and subgrade.

During thaw periods, the pavement structure below the PCC layer thaws and can become saturated with water from the melting ice lenses and infiltration of surface water from rain or melting snow. This saturation of the material reduces the strength of the base, subbase or subgrade, or all three, leading to reduced bearing capacity of the entire pavement structure. In addition, the large temperature differentials during thawing periods can cause curling of the corners and edges of slabs of PCC pavements, thus affecting load transfer across joints.

The objective of the study was to determine any structural changes in PCC airport pavements during thaw-weakening periods. To evaluate these changes, CRREL conducted Falling Weight Deflectometer (FWD) measurements to quantify the changes in the stiffness of the pavement structure and the load transfer efficiency of the joints. In addition, subsurface pavement temperatures were measured at selected locations at each airport. This report gives a general description of the airports and the pavement structures and a comprehensive analysis of the FWD measurements.

DESCRIPTION OF AIRFIELDS

Central Wisconsin Airport (CWA)

CWA is located in Mosinee, Wisconsin (Fig. 1). The subsurface soils at CWA are silts, sandy silts and clayey silts and can be classified as either SM or ML using the Unified Soil Classification System, and as F3 and F4 with respect to frost-susceptibility (Stark and Berg 1989). F3 and F4 soils are very susceptible to frost heave and thaw weakening. Stark and Berg (1989) also reported that the subgrade was not uni-

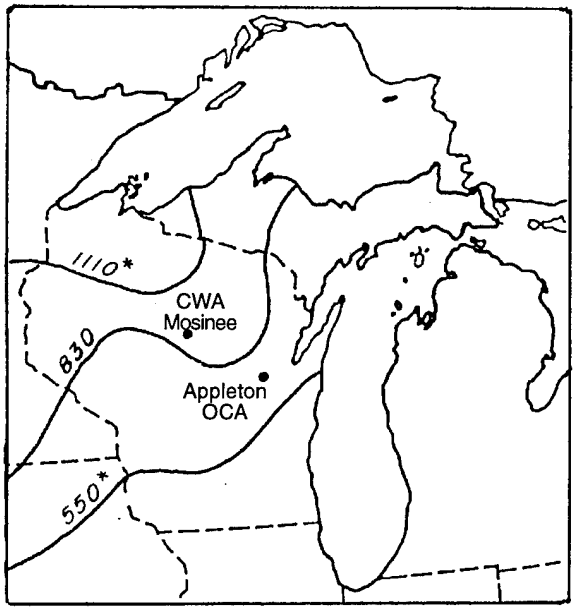

* Mean Air Freezing Index (°C-days)

Figure 1. Location of airfields.

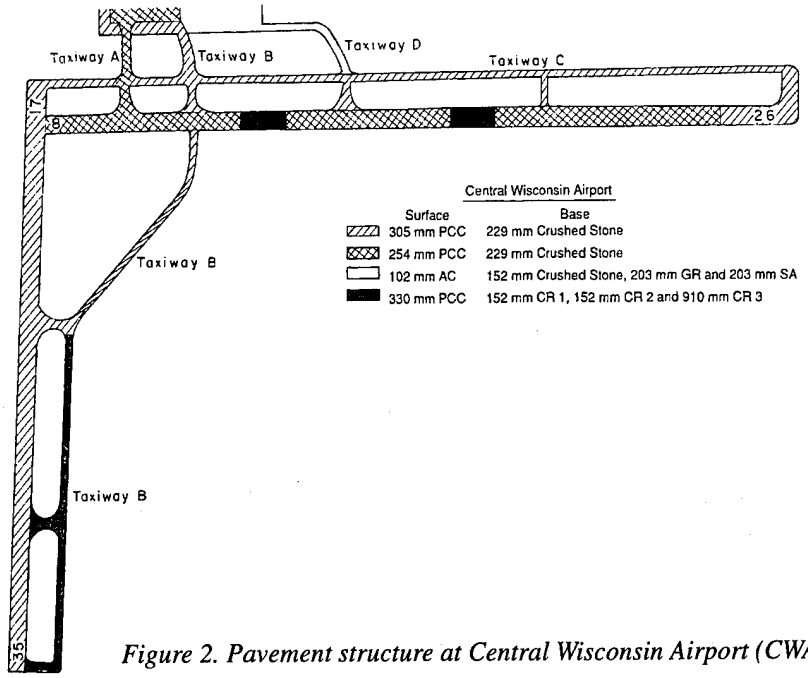

Figure 2. Pavement structure at Central Wisconsin Airport (CWA).

form, having clusters of rocks and boulders incorporated into the finer grained soils. Bedrock was reported at uneven depths and at some locations it was close to the pavement surface.

The airport pavements consist of two intersecting runways, five taxiways and three ramps (Fig. 2). The original airfield—runway 8/26, taxiway A and an air carrier ramp—was constructed in 1968 and 1969. Between 1972 and 1973, runway 17/35 and taxiways C, D and E were constructed. Also in 1973, runway 8/26 was extended by 245 m and the air carrier ramp expanded. Taxiway B (between the ramp and taxiway C) was constructed in 1975 and was extended to connect the two runways in 1977. Portions of runway 8/26 were reconstructed in 1987. A summary of the construction history, length, width and types of joints of the different pavement structures at CWA is presented in Table 1.

The airfield basically was constructed with PCC. The original runway, taxiway and ramp, constructed

Table 1. Pavement structures at Central Wisconsin Airport.

Pavement	*Date constructed*	*Length (m)*	*Width (m)*	*Slab size (m)*	*Longitudinal joint*	*Transverse joint*
Runway 8/26 (original)	1968	2042	46	3.8 × 6.1	keyed & dummy	doweled
Runway 8/26 (extension)	1973	244	46	7.6 × 7.6	keyed	doweled
Runway 17/35	1972	1737	46	7.6 × 7.6	keyed	doweled
Taxiway A	1969	297	23	3.8 × 6.1	keyed & tied	doweled
Taxiway B (ramp to taxiway C)	1975	139	23	7.6 × 7.6 3.8 × 7.6	keyed & tied	doweled
Taxiway B (taxiway C to 17/35)	1977	.954	15	3.8 × 7.6	Butt, tied	doweled & dummy
Taxiway C	1973	2256	15	7.6 × 7.6 3.8 × 7.6	keyed & tied	doweled
Taxiway D	1973	88	20	7.6 × 7.6 3.8 × 7.6	keyed & tied	doweled
Taxiway E	1973	88	20	3.8 × 5.3	keyed & tied	doweled

in 1968 and 1969, had 254 mm of PCC over 229 mm of crushed stone base over subgrade. Later construction mostly used 305 mm of PCC over 229 mm of crushed stone base over subgrade. The structure of the different pavement sections as of spring 1986 is also shown in Figure 2.

The slabs sizes were primarily 7.6 by 7.6 m; however, in some areas, the slabs were 3.8 by 3.8 m. Other sizes used are shown in Table 1. Loads are transferred across the transverse joints by dowels and aggregate interlocks (Table 1) (CMT 1984). At longitudinal joints, loads are transferred through keyways, aggregate interlocks and tiebars (Table 1) (CMT 1984). The primary types of aircraft using the airport are Convair 580 (24,766 kg), MD DC-9 (44,452 kg) and Boeing 757 (115,666 kg) (CMT 1984).

was a heavy clay (USC classification–CL; FAA classification–E7) with a design California Bearing Ratio (CBR) of 4. They also reported clay migration into the base course and trapped water under the pavement.

The airport pavements consist of two intersecting runways, five taxiways and three ramps (Fig. 3). Runway 3/21 was constructed in 1967 and 1968, with 203 mm of PCC (254 mm in critical areas) over 203 mm of crushed gravel over subgrade. Runway 11/29, reconstructed in 1988 and 1989, had 178 mm PCC (229 mm in critical areas) over 203 mm of crushed aggregate base course over subgrade.

The PCC slabs were mostly 3.8 m wide by 6.1 m long; but, in some areas, the slabs were 3.8 m wide by 5.3 m long. A typical transverse joint used aggregate interlocks and dowels for load transfer.* Across longi-

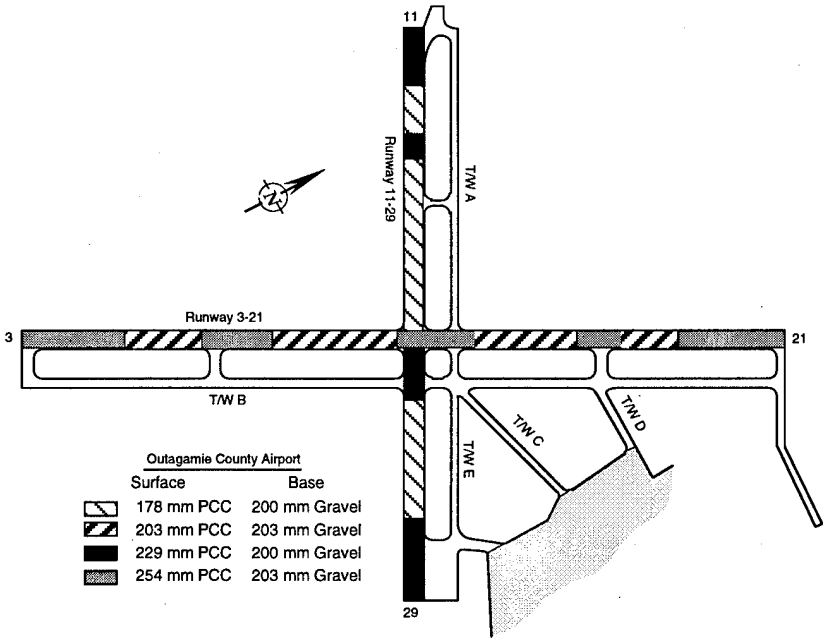

Figure 3. Pavement structure at Outagamie County Airport (OCA).

Outagamie County Airport (OCA)

OCA is located near Appleton, Wisconsin (Fig. 1). The subgrade at the airport consists mostly of a low plasticity clay (CL), some sand (SP) and silty sand (SM). At OCA, bedrock was estimated to be 4.0 m deep or more, on the basis of boring logs. ERES consultants (1985) reported the subgrade under runway 3/21 as a highly frost-susceptible red silty clay. They also reported that the subbase material may be frost-susceptible because of a high amount of fines passing the no. 200 sieve (8–10 %). Runway 3/21 has severe frost heave problems (ERES 1985). Mead and Hunt (1988) reported that the subgrade under runway 11/29

tudinal joints, keyways, aggregate interlocks and tiebars were used for load transfer (ERES Consultants 1985, Mead and Hunt 1988). Richardson stated that on the basis of a pavement evaluation done prior to 1986, the gross allowable aircraft weights on runway 11/29 were 27,200-kg single, 40,800-kg dual and 74,860-kg dual tandem. On runway 3/21, the gross allowable aircraft weights were 38,570-kg single, 81,670-kg dual and 95,280-kg dual tandem.

* Personal Communication, with K. Richardson, Wisconsin Department of Transportation, 1991.

FIELD INSTRUMENTATION AND TESTING PROGRAM

In the summer of 1985, several locations along the airport runways and taxiways were instrumented with moisture sensors and copper-constantan thermocouples as temperature sensors. At CWA, six locations were instrumented for temperature measurement (Fig. 4a). At OCA, there were two temperature measurement sites (Fig. 4b). With a few exceptions, thermocouples were placed to depths of approximately 5 m below the pavement surface. The spacings of the sensors are given in Table 2. At TC4, the hole could not be held open past 2.5 m from the surface.

The temperature measurements were made periodically by airport personnel during the winter months and by CRREL personnel during the FWD testing period in the spring. The measured temperatures at the two airports are given in Janoo and Berg (1996).

In the spring of 1986, non-destructive testing using a Dynatest 8000 Falling Weight Deflectometer (FWD) was conducted at selected sites at the two airports. The FWD test sites covered a large area of the airports and included both AC and PCC pavements. As mentioned earlier, the analysis presented here is for only the PCC slabs. Deflection measurements were made

Table 2. Temperature sensor locations under pavement surface (cm).

Sensor no.	*TC1, TC2 (CWA) TC1, TC2 (OCA)*	*TC3 (CWA)*	*TC4 (CWA)*
1	30.5	30.5	30.5
2	45.7	45.7	45.7
3	61	106.7	61
4	91.4	137.2	91.4
5	121.9	167.6	121.9
6	152.4	198.1	152.4
7	182.9	228.6	182.9
8	213.4	259.1	213.4
9	243.8	289.6	243.8
10	304.8	350.5	259.1
11	365.8	411.5	137.2
12	487.7	472.4	106.7

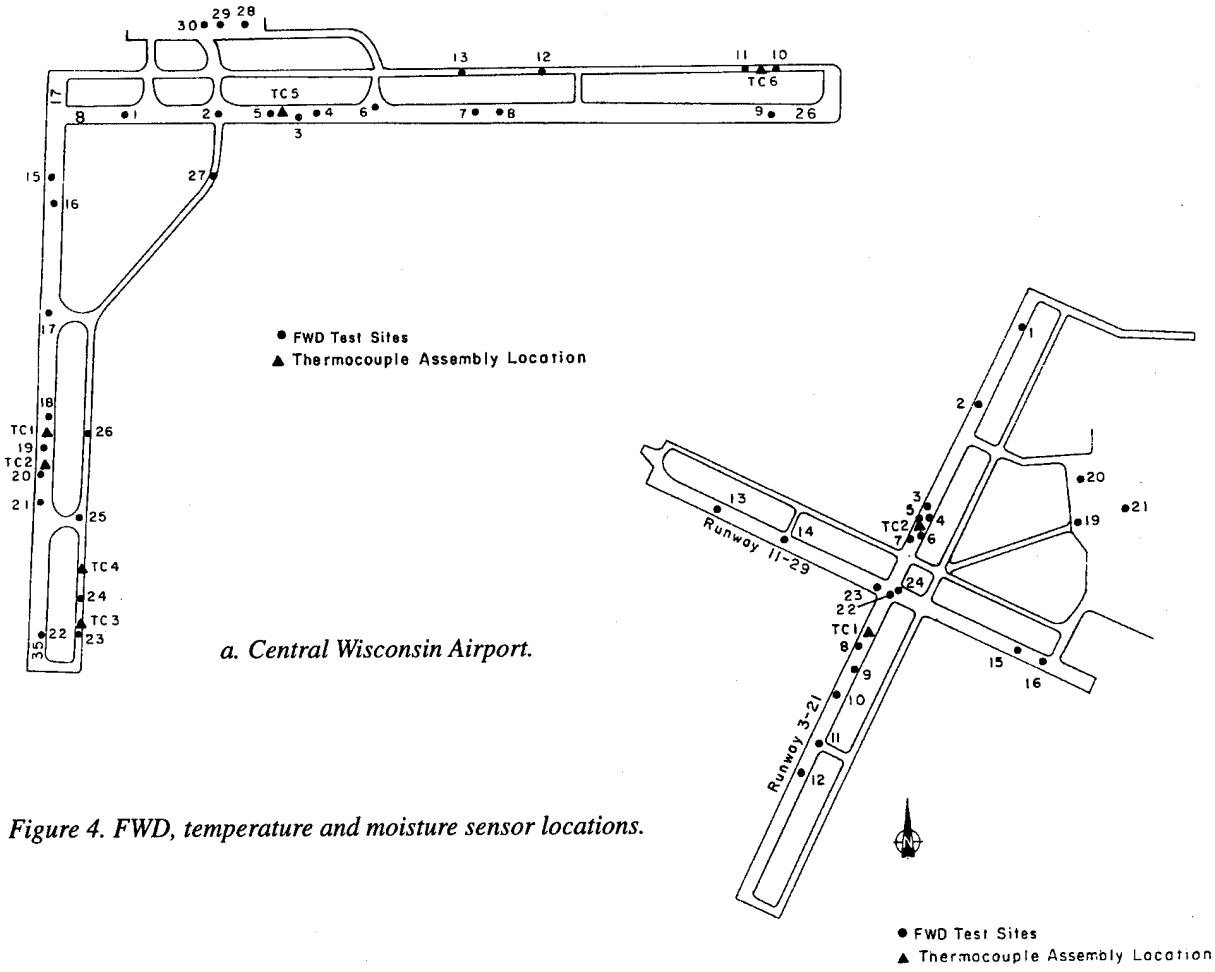

a. Central Wisconsin Airport.

b. Outagamie County Airport.

Figure 4. FWD, temperature and moisture sensor locations.

at the center of the slab, at transverse joints, longitudinal joints and at a corner. The FWD test program consisted of one drop at each of four height levels producing loads of 600, 900, 1100 and 1600 kN, respectively, on the pavement surface. The deflection sensors were located at 0, 300, 600, 900, 1200, 1500 and 1800 mm from the center of the loading plate. The FWD loading plate used was 300 mm in diameter. The location of the FWD tests at the two airports are shown in Figure 4.

ENVIRONMENTAL DATA ANALYSIS

The environmental data used in this analysis were the air temperature and subsurface temperatures. The daily maximum and minimum air temperature at the airports between 1 October 1985 and 30 April 1986 are presented in Figure 5. The air temperature data used at CWA were obtained from the nearest weather station, which was located approximately 24 km north of the airport at Wausau, since there was no meteorological station at CWA. These air temperatures were used to determine air-freezing indices (Fig. 6). The air-freezing index was calculated in Celsius degree-days using

$$\text{Air-freezing index} = \sum_{n=1}^{181} \frac{T_{max} + T_{min}}{2}$$

where T_{max} = daily maximum temperature (°C)
T_{min} = daily minimum temperature(°C)
$(n = 1)$ = 1 October 1985
$n = 181$ = 30 April 1986.

The air-freezing index range was 1100 and 920°C days at CWA and OCA respectively. The design freez-

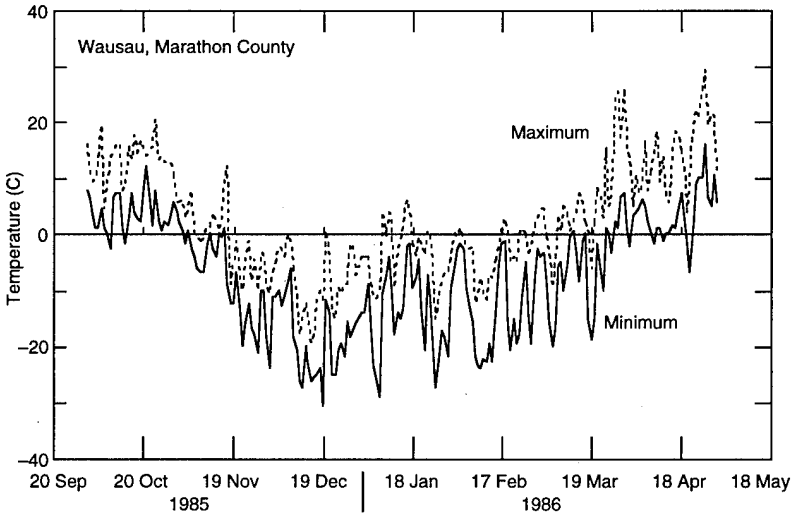

a. Central Wisconsin Airport.

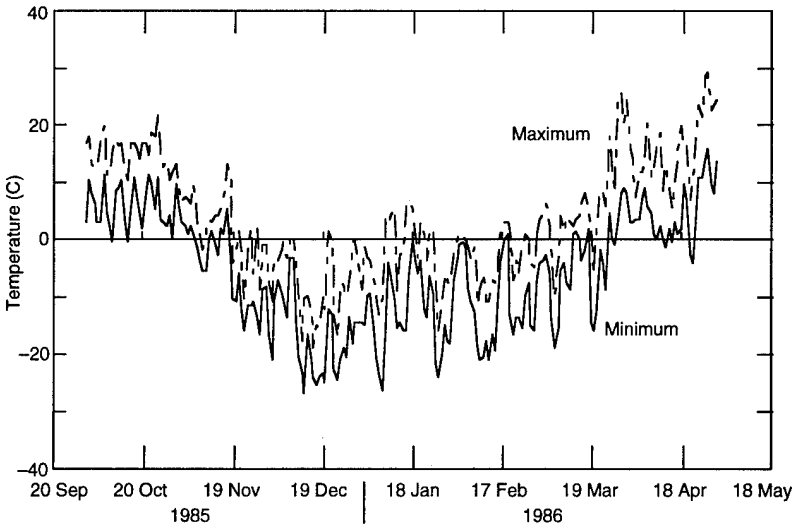

b. Outagamie County Airport, Appleton.

Figure 5. Daily maximum and minimum temperatures.

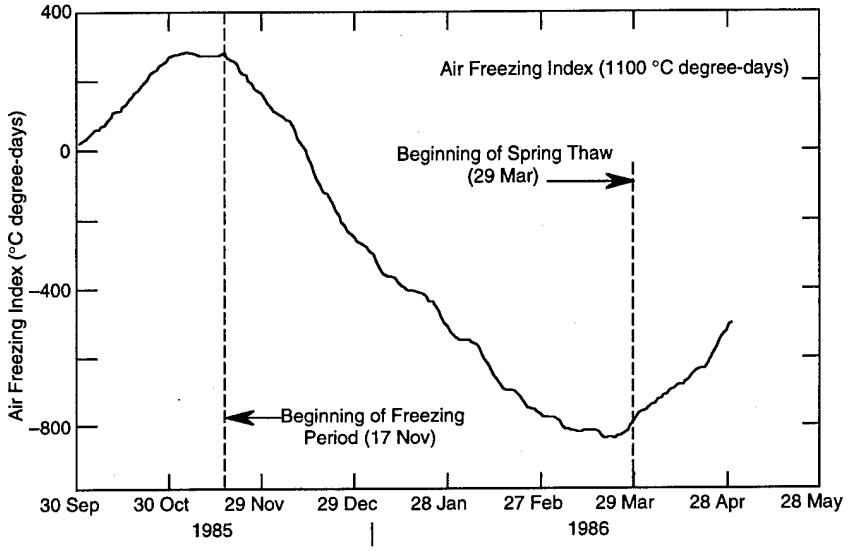

a. Central Wisconsin Airport.

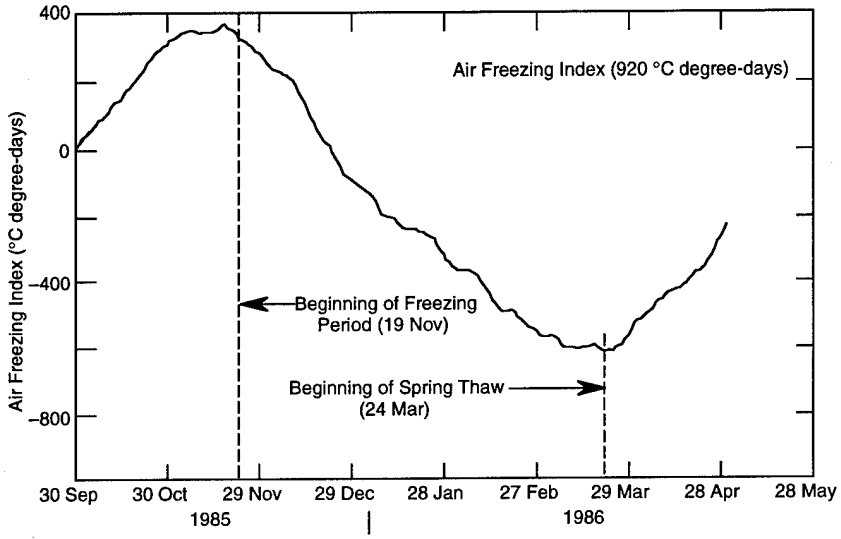

b. Outagamie County Airport.

Figure 6. Air-freezing indices.

ing index published in Army TM 5-818-2 for these areas ranges between 830 and 1110°C days, which means that the air-freezing index in the winter of 1985–1986 was close to that. The air-freezing season, as indicated in the above two figures, ended around 24 March 1986 at OCA and 29 March 1986 at CWA.

Using the temperature measurements gathered from the various thermocouple locations, we determined frost and thaw depth, which we assumed to be where the temperature was 0°C. Frost depths at the beginning of the winter were calculated for some of the locations and are also presented in Janoo and Berg (1966). A summary of the frost and thaw penetration depths at CWA and OCA is presented in Figure 7. The maximum measured frost penetration at CWA ranged around 2000 mm and at OCA around 1300 mm. The measured subsurface temperatures indicate that thaw began at CWA around 29 March. The ground was completely thawed by the second week of April. At OCA, when subsurface temperature measurements were made in the spring, thaw had already started. The ground was completely thawed by the first week of April.

FWD DATA ANALYSIS

Falling weight deflection measurements were conducted at four locations on a slab. These were at 1) the middle, 2) across the transverse joint, 3) across the longitudinal joint and 4) across the diagonal on one

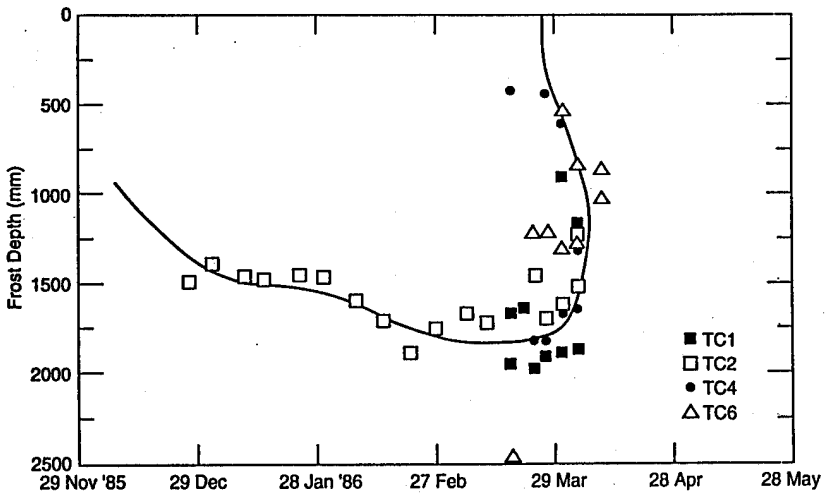

a. Central Wisconsin Airport.

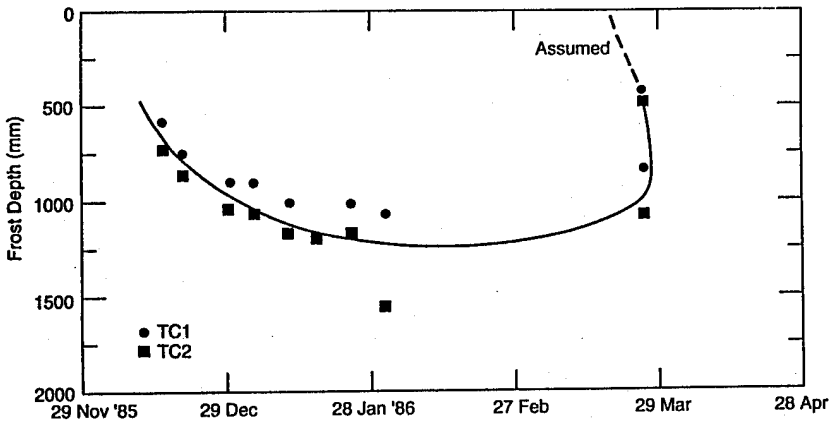

b. Outagamie County Airport.

Figure 7. Frost and thaw depths calculated from subsurface temperature measurements.

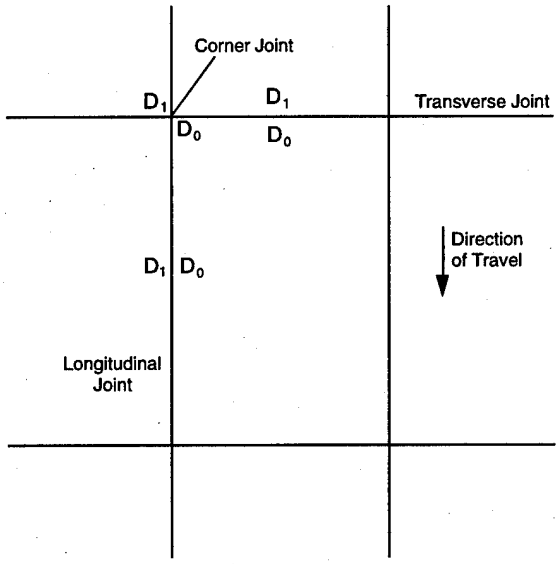

Figure 8. Location of FWD sensors across joints and corner of a PCC slab.

corner of the slab. The placement of the sensors across the joints and corner is illustrated in Figure 8. The FWD measurements were alternated between the two airports. At CWA, FWD deflection measurements began on 18 March and continued to 24 April 1986 (Table 3a). At OCA, FWD testing started on 15 March and continued to 26 April 1986 (Table 3b). The FWD deflection measurements taken at both airports are presented in Janoo and Berg (1966).

The pavement surface temperatures at the time of FWD testing for both airports are presented in Table 4. Surface temperatures were measured with a thermocouple attached to a wooden dowel. The thermocouple was placed against the pavement by the FWD operator. At the time of FWD testing, the pavement surface at CWA was dry except on 18 March and 14 April. At OCA, the pavement surface was dry except on 5 April. Subsurface temperature measurements indicated that the pavement structures at CWA were frozen at the beginning of FWD testing and completely thawed by the

Table 3. Types of FWD tests conducted.

a. Central Wisconsin Airport.

Date	1	2	3	4	5	6	7	8	9	10
18 Mar 86	—	—	—	—	—	—	—	—	—	1,2,3,4
20 Mar 86	1,2,3,4	1,2,3,4	1,2,3,4	1,2,3,4	1,2,3,4	1,2,3,4	1,2,3,4	1,2,3,4	1,2,3,4	—
24 Mar 86	1,2,3,4	1,2,3,4	1,2,3,4	1,2,3,4	1,2,3,4	1,2,3,4	1,2,3,4	1,2,3,4	1,2,3,4	1,2,3,4
27 Mar 86	1,2	1,2	1,2	1,2	1,2	1,2	1,2	1,2	1,2	1,2
4 Apr 86	1,2,3,4	1,2,3,4	1,2,3,4	1,2,3,4	1,2,3,4	1,2,3,4	1,2,3,4	1,2,3,4	1,2,3,4	1,2,3,4
7 Apr 86	1,2,3,4	1,2,3,4	1,2,3,4	1,2,3,4	1,2,3,4	1,2,3,4	1,2,3,4	1,2,3,4	1,2,3,4	1,2,3,4
10 Apr 86	1,2	1,2	1,2	1,2	1,2	1,2	1,2	1,2	1,2	1,2
14 Apr 86	1,2	1,2	1,2	1,2	1,2	1,2	1,2	1,2	1,2	1,2,3,4
17 Apr 86	1,2,3,4	1,2,3,4	1,2,3,4	1,2,3,4	1,2,3,4	1,2,3,4	1,2,3,4	1,2,3,4	1,2,3,4	1,2
21 Apr 86	1,2,3,4	1,2,3,4	1,2,3,4	1,2,3,4	1,2,3,4	1,2,3,4	1,2,3,4	1,2,3,4	1,2,3,4	1,2,3,4
24 Apr 86	1,2	1,2	1,2	1,2	1,2	1,2	1,2	1,2	1,2	1,2

Date	11	12	13	14	15	16	17	18	19	20
18 Mar 86	1,2,3,4	1,2	1,2,3,4	—	1,2,3,4	1,2,3,4	1,2,3,4	1,2,3,4	1,2,3,4	1,2,3,4
20 Mar 86	—	—	—	—	—	—	—	—	—	—
24 Mar 86	1,2	1,2	1,2,3,4	—	1,2,3,4	1,2,3,4	1,2,3,4	1,2,3,4	1,2,3,4	1,2,3
27 Mar 86	1,2	1,2	1,2	—	1,2	1,2	1,2	1,2	1,2	1,2,3,4
4 Apr 86	1,2	1,2	1,2,3,4	—	1,2,3,4	1,2,3,4	1,2,3,4	1,2,3,4	1,2,3,4	1,2,3,4
7 Apr 86	1,2	1,2	1,2,3,4	—	1,2,3,4	1,2,3,4	1,2,3,4	1,2,3,4	1,2,3,4	1,2,3,4
10 Apr 86	1,2	1,2	1,2	—	1,2	1,2	1,2	1,2	1,2	1,2
14 Apr 86	1,2	1,2	1,2,3	—	1,2,3,4	1,2,3,4	1,2,3,4	1,2,3,4	1,2,3,4	1,2,3,4
17 Apr 86	1,2	1,2	1,2	—	1,2	1,2	1,2	1,2	1,2	1,2
21 Apr 86	1,2	1,2	1,2,3	—	1,2	1,2	1,2	1,2	1,2	1,2
24 Apr 86	1,2	1,2	1,2	—	1,2	1,2	1,2	1,2	1,2	1,2

Date	21	22	23	24	25	26	27
18 Mar 86	1,2,3,4	1,2,3,4	1,2,3,4	1,2,3,4	1,2,3,4	1,2,3,4	1,2
20 Mar 86	—	—	—	—	—	—	—
24 Mar 86	—	—	—	—	—	—	—
27 Mar 86	1,2,3,4	1,2,3,4	1,2,3,4	1,2,3,4	1,2,3,4	1,2,3,4	1,2
4 Apr 86	1,2,3,4	1,2,3,4	1,2,3,4	1,2,3,4	1,2,3,4	1,2,3,4	1,2
7 Apr 86	1,2,3,4	1,2,3,4	1,2,3,4	1,2,3,4	1,2,3,4	1,2,3,4	1,2
10 Apr 86	1,2	1,2	1,2	1,2	1,2	1,2	1,2
14 Apr 86	1,2,3,4	1,2,3,4	1,2,3,4	1,2,3,4	1,2,3,4	1,2,3,4	1,2
17 Apr 86	1,2	1,2	1,2	1,2	1,2	1,2	1,2
21 Apr 86	1,2	1,2	1,2,3,4	1,2,3,4	1,2,3,4	1,2,3,4	1,2
24 Apr 86	1,2	1,2	1,2	1,2	1,2	1,2	1,2

b. Outagamie County Airport.

Date	1	2	3	4	5	6	7	8	9	10	11
15 Mar 86	1,2,3,4	1,2,3,4	1,2,3,4	1,2,3,4	1,2,3,4	1,2,3,4	1,2,3,4	1,2,3,4	1,2,3,4	1,2,3,4	1,2,3,4
26 Mar 86	1,2	1,2	1,2	1,2	1,2	1,2	1,2	1,2	1,2	1,2	1,2
29 Mar 86	1,2,3,4	1,2,3,4	1,2,3,4	1,2,3,4	1,2,3,4	1,2,3,4	1,2,3,4	1,2,3,4	1,2,3,4	1,2,3,4	1,2,3,4
5 Apr 86	1,2,3,4	1,2,3,4	1,2,3,4	1,2,3,4	1,2,3,4	1,2,3,4	1,2,3,4	1,2,3,4	1,2,3,4	1,2,3,4	1,2,3,4
9 Apr 86	1,2	1,2	1,2	1,2	1,2	1,2	1,2	1,2	1,2	1,2	1,2
12 Apr 86	1,2,3,4	1,2,3,4	1,2,3,4	1,2,3,4	1,2,3,4	1,2,3,4	1,2,3,4	1,2,3,4	1,2,3,4	1,2,3,4	1,2,3,4
16 Apr 86	1,2	1,2	1,2	1,2	1,2	1,2	1,2	1,2	1,2	1,2	1,2
23 Apr 86	1,2	1,2	1,2	1,2	1,2	1,2	1,2	1,2	1,2	1,2	1,2
26 Apr 86	1,2,3,4	1,2,3,4	1,2,3,4	1,2,3,4	1,2,3,4	1,2,3	1,2,3,4	1,2,3,4	1,2,3,4	1,2,3,4	1,2,3,4

Date	12	13	14	15	16	19	20	21	22	23	24
15 Mar 86	1,2,3,4	1,2,3,4	1,2,3,4	1,2,3,4	1,2,3,4	1,2,3,4	1,2,3,4	1,2,3,4	1,2,3,4	1,2,3,4	1,2,3,4
26 Mar 86	1,2	1,2	1,2	1,2	1,2	1,2	1,2	1,2	1,2	1,2	1,2
29 Mar 86	1,2,3,4	1,2,3,4	1,2,3,4	1,2,3,4	1,2,3,4	1,2,3,4	1,2,3,4	1,2,3,4	1,2,3,4	1,2,3,4	1,2,3,4
5 Apr 86	1,2,3,4	1,2,3,4	1,2,3,4	1,2,3,4	1,2,3,4	1,2,3,4	1,2,3,4	1,2,3,4	1,2,3,4	1,2,3,4	1,2,3,4
9 Apr 86	1,2	1,2	1,2	1,2	1,2	1,2	1,2	1,2	1,2	1,2	1,2
12 Apr 86	1,2,3,4	1,2,3,4	1,2,3,4	1,2,3,4	1,2,3,4	1,2,3,4	1,2,3,4	1,2,3,4	1,2,3,4	1,2,3,4	1,2,3,4
16 Apr 86	1,2	1,2	1,2	1,2	1,2	1,2	1,2	1,2	1,2	1,2	1,2
23 Apr 86	1,2	1,2	1,2	1,2	1,2	1,2	1,2	1,2	1,2	1,2	1,2

1–Center of slab; 2–Transverse joint; 3–Longitudinal joint; 4–Corner.

Table 4. Pavement surface temperatures (°C) at times of FWD tests.

a. Central Wisconsin Airport.

Date	1	2	3	4	5	6	7	8	9	10
18 Mar 86	—	—	—	—	—	—	—	—	—	2.2
20 Mar 86	–1.1	–1.7	–2.8	–2.8	–2.8	–2.8	–2.8	–2.8	–2.8	—
24 Mar 86	1.1	1.7	1.7	2.2	1.1	2.8	2.2	2.2	3.3	2.8
27 Mar 86	8.9	8.9	6.7	5.6	7.2	5.6	6.1	6.1	5.0	6.7
4 Apr 86	11.1	12.2	11.7	4.4	11.7	4.4	4.4	4.4	4.4	11.7
7 Apr 86	20.0	20.0	15.6	15.6	15.6	15.6	15.6	18.9	18.9	18.9
10 Apr 86	11.1	8.3	8.3	8.3	8.3	7.2	7.2	7.2	7.2	8.9
14 Apr 86	2.8	2.8	2.2	2.8	2.8	2.8	2.8	2.8	2.8	4.4
17 Apr 86	12.2	11.1	13.3	12.8	13.3	13.3	13.9	14.4	14.4	16.1
21 Apr 86	0.6	0.6	0.6	0.6	0.6	0.6	2.2	2.2	1.7	1.7
24 Apr 86	16.1	16.1	16.1	16.7	16.1	16.7	17.2	18.3	18.3	18.9

Date	11	12	13	14	15	16	17	18	19	20
18 Mar 86	2.2	2.2	2.2	—	6.1	6.1	3.3	2.2	1.7	1.7
20 Mar 86	—	—	—	—	—	—	—	—	—	—
24 Mar 86	2.2	3.3	3.9	—	5.6	5.0	4.4	4.4	5.0	2.2
27 Mar 86	7.8	8.3	9.4	—	10.0	10.0	12.8	11.7	12.8	13.3
4 Apr 86	12.2	11.7	11.7	—	10.0	8.9	8.9	10.0	9.4	9.4
7 Apr 86	18.9	18.9	18.9	—	19.4	18.9	19.4	18.9	18.9	18.9
10 Apr 86	11.1	11.1	12.2	—	17.2	17.2	16.1	16.1	15.6	16.7
14 Apr 86	5.0	4.4	3.9	—	8.3	6.1	5.6	5.0	5.0	5.6
17 Apr 86	17.8	17.8	17.8	—	18.9	18.9	18.3	18.3	18.3	18.3
21 Apr 86	3.9	3.3	4.4	—	8.9	8.9	8.9	9.4	8.9	8.3
24 Apr 86	19.4	20.0	20.6	—	25.0	25.0	23.3	23.9	25.6	26.7

Date	21	22	23	24	25	26	27	28	29	30
18 Mar 86	1.7	1.7	1.7	1.7	1.7	1.7	2.2	3.3	3.3	3.3
20 Mar 86	—	—	—	—	—	—	—	—	—	—
24 Mar 86	—	—	—	—	—	—	—	6.1	4.4	4.4
27 Mar 86	13.3	11.7	11.7	12.8	13.3	12.8	10.0	14.4	14.4	12.2
4 Apr 86	9.4	9.4	11.7	11.7	12.2	13.3	13.3	12.8	12.8	12.2
7 Apr 86	18.3	19.4	18.9	20.0	21.7	19.4	22.8	21.7	21.7	21.7
10 Apr 86	16.1	15.6	15.6	16.1	16.7	16.7	16.1	16.1	20.6	20.6
14 Apr 86	6.7	5.6	5.6	5.6	5.6	5.6	5.0	4.4		
17 Apr 86	18.3	18.3	18.3	18.9	19.4	19.4	19.4	22.2	21.7	21.7
21 Apr 86	8.9	9.4	7.8	7.8	7.8	8.9	8.9	11.1	11.7	11.7
24 Apr 86	27.2	25.6	20.6	20.6	20.0	21.1	20.6	26.1	26.1	26.1

b. Outagamie County Airport.

Date	1	2	3	4	5	6	7	8	9	10	11
15 Mar 86	2.8	4.4	3.3	6.1	3.3	7.2	4.4	4.4	4.4	4.4	6.7
26 Mar 86	11.1	11.1	11.1	12.2	11.7	13.9	15.6	16.1	16.1	16.1	16.7
29 Mar 86	21.1	21.7	23.3	23.9	23.9	25.6	25.6	23.9	23.9	25.0	25.0
5 Apr 86	10.0	10.0	9.4	9.4	10.0	10.0	10.6	10.6	11.1	11.1	12.2
9 Apr 86	7.8	9.4	10.0	9.4	10.0	10.0	10.6	10.6	10.6	10.6	11.1
12 Apr 86	6.7	7.2	7.2	7.2	7.2	7.2	8.9	8.3	7.8	7.8	7.8
16 Apr 86	7.8	7.8	8.3	8.3	8.3	8.9	8.9	8.9	8.9	8.9	10.0
23 Apr 86	16.7	16.7	16.1	17.2	17.2	17.2	17.8	17.8	17.8	17.8	19.4
26 Apr 86	23.3	23.3	23.3	23.3	23.9	23.9	24.4	24.4	24.4	24.4	24.4

Date	12	13	14	15	16	19	20	21	22	23	24
15 Mar 86	4.4	4.4	4.4	4.4	4.4	4.4	4.4	4.4	3.9	5.6	5.6
26 Mar 86	16.7	12.2	10.6	12.8	13.3	13.3	12.2	10.6	15.6	11.1	11.1
29 Mar 86	25.0	22.2	23.3	23.3	23.3	26.7	27.2	27.2	27.2	25.6	25.6
5 Apr 86	11.7	10.6	10.0	10.0	8.9	10.0	10.0	10.0	10.6	10.0	10.0
9 Apr 86	10.6	8.9	8.3	9.4	10.0	8.3	8.9	10.0	10.6	8.9	9.4
12 Apr 86	8.3	6.1	6.1	7.2	6.7	10.0	9.4	9.4	9.4	6.7	6.7
16 Apr 86	11.1	8.3	8.3	11.1	11.1	11.1	11.1	10.6	6.7	8.3	8.3
23 Apr 86	18.9	13.3	13.9	15.0	15.0	18.9	18.9	19.4	17.8	14.4	14.4
26 Apr 86	25.0	27.8	26.1	27.8	27.8	—	—	—	26.7	26.7	26.7

end. At OCA the subsurface temperature measurements indicated that the pavement structures were partially thawed at the beginning of FWD testing and completely thawed prior to the end. It should be noted that no FWD data were obtained during the 6-day period from 29 March through 4 April, which was undoubtedly the critical thaw-weakening period. This was unfortunate; however, we will work with the data that we have.

Bearing capacity analysis

Any change in the structural capacity of the pavement during the thaw-weakening period was inferred from the FWD data. We used both the deflection basin area concept and the Impulse Stiffness Modulus (ISM) to characterize the changes in pavement performance. The basin area method was a good indicator of AC pavement response during thaw periods under controlled conditions (Janoo and Berg 1990, 1991). The deflection basin obtained from the seven-deflection sensor system is used to calculate the basin area by the following equation

$$\text{Basin Area} = \frac{1}{2}\sum_{i=0}^{6}\left[(\delta_i + \delta_{i+1})(r_{i+1} - r_i)\right]$$

where δ_i is deflection at sensor (i), and r_i is sensor (i) distance from the center of the loading plate.

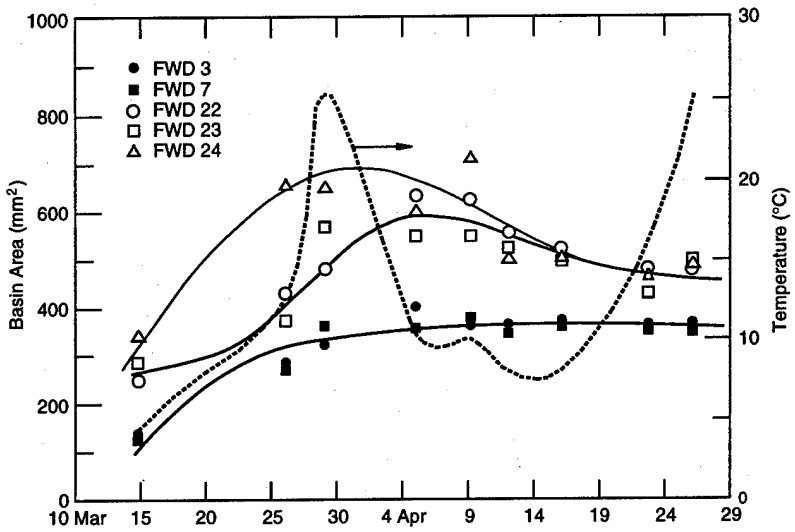

a. Change in basin area.

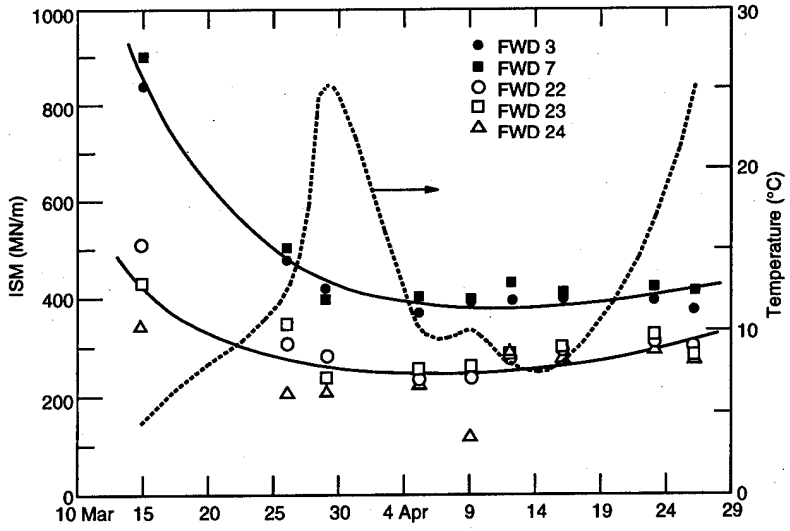

b. Change in ISM.

Figure 9. Changes in basin area and impulse stiffness modulus during spring thaw at Outagamie County Airport.

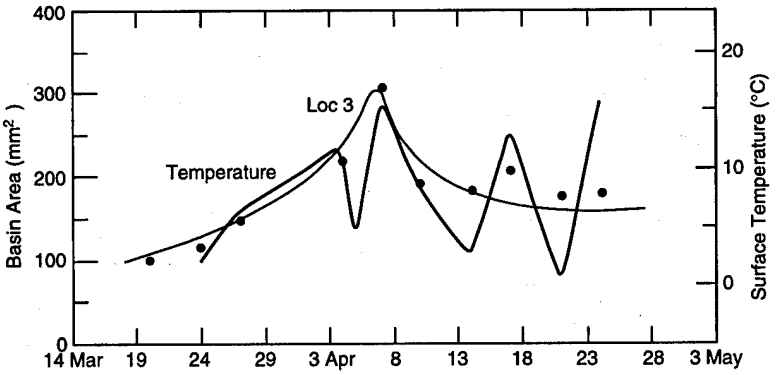

a. FWD location 3 .

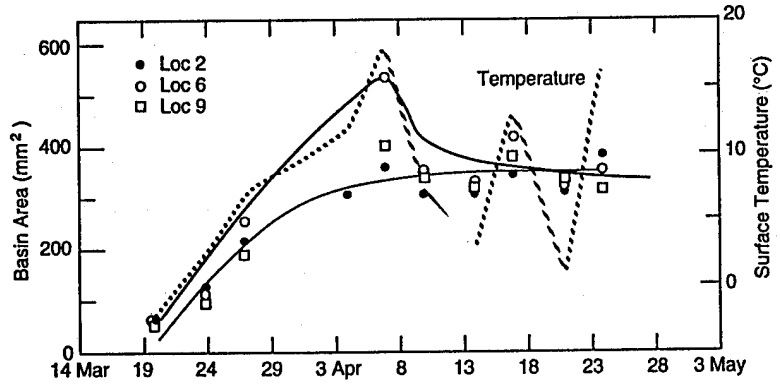

b. FWD locations 2, 6 and 9.

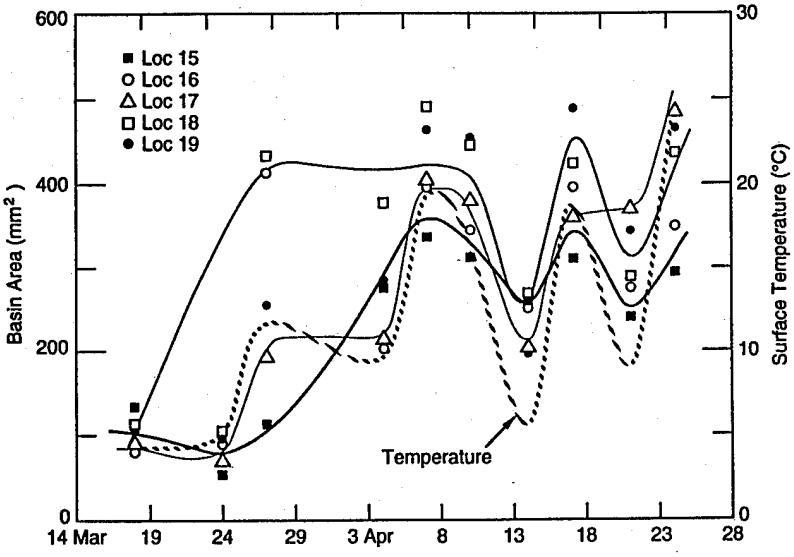

c. FWD locations 15 to 19.

Figure 10. Changes in basin area during spring thaw at Central Wisconsin Airport.

The ISM, used by the Corps of Engineers for characterizing pavement structures, is analogous to the spring constant (k) of a spring mass system. The ISM is calculated from

$$\text{ISM} = \frac{P}{\delta_0}$$

where P is applied FWD load and δ_0 is deflection under the center of the plate.

Typical changes in ISM values and basin areas at the centers of selected slabs are presented in Figures 9–11. The measured surface temperatures at the FWD sites are also plotted in these figures.

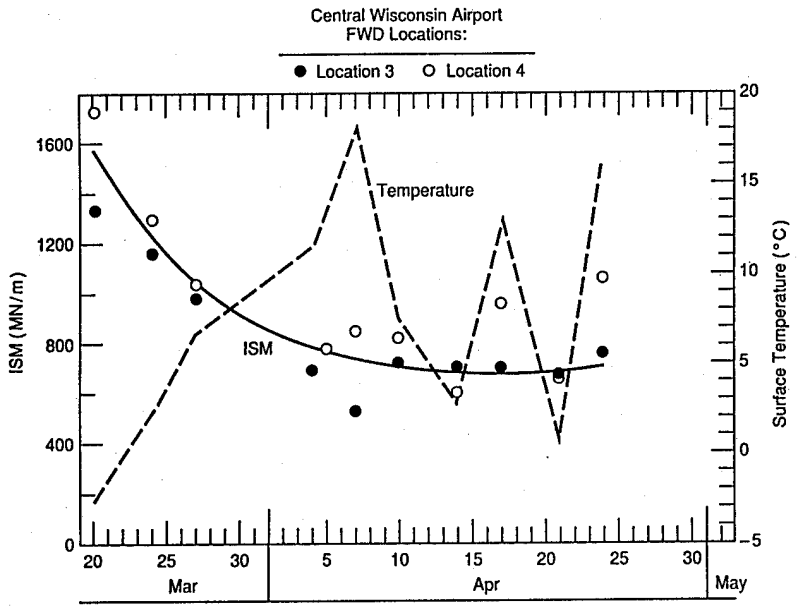

a. FWD locations 3 and 4.

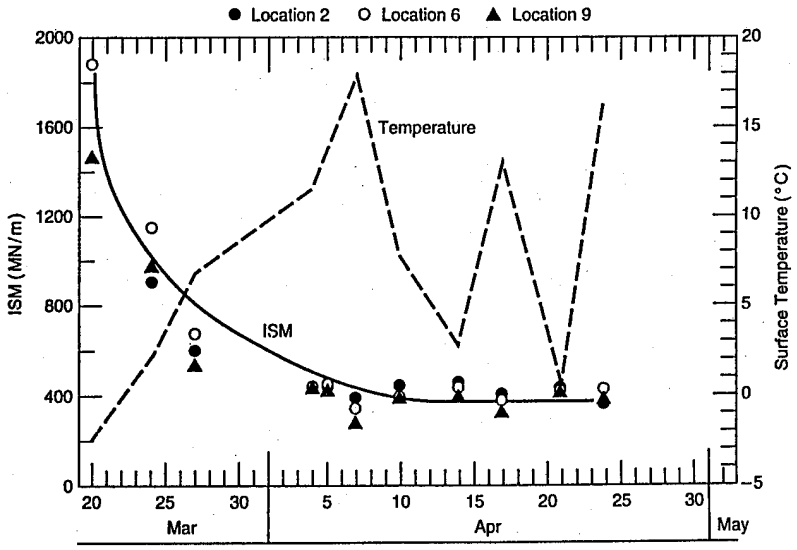

b. FWD locations 2, 6 and 9.

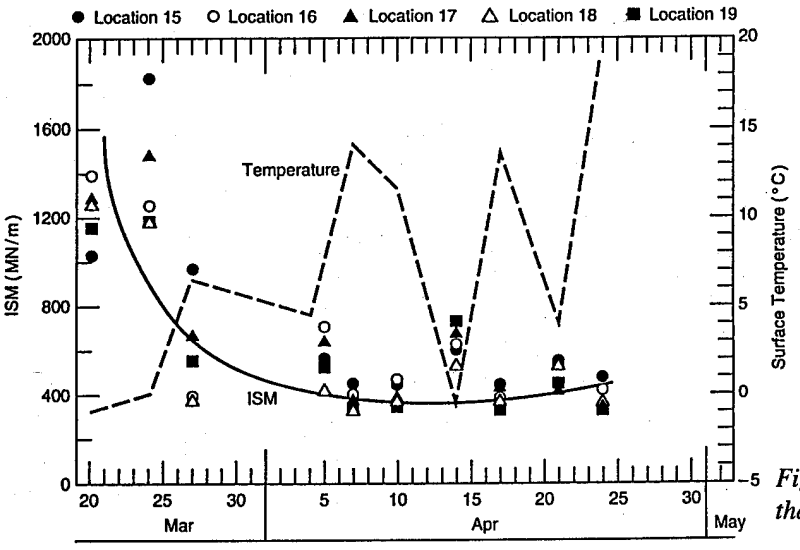

c. FWD locations 15 to 19.

Figure 11. Changes in ISM during spring thaw at Central Wisconsin Airport.

Outagamie County Airport

At the beginning of spring thaw, the basin areas are low, indicating a stiff pavement structure. As expected, we observed that as the pavement structure thawed, the basin areas increased. As mentioned above, we have used plots of the deflection basin area versus time to identify periods of thaw weakening and recovery.

At FWD locations 3 and 7 (Fig. 9a), the basin areas increase somewhat at the beginning of thaw and then level off after 5 April. This suggests that the pavement structure at these locations does not undergo substantial thaw weakening. However, at other locations, such as FWD sites 22, 23 and 24, the pavement structure undergoes more substantial thaw weakening and recovery, as shown by the shape of the basin area curves in Figure 9a. If total recovery is assumed to occur on 23 April, the bearing capacity of the pavement structure at locations 22, 23 and 24 was reduced by 30 to 40%.

The changes in the ISM can also be used to identify periods of thaw weakening and recovery. The changes in ISM with time for the same FWD locations discussed previously are shown in Figure 9b. At the beginning of spring thaw, the value of the ISM is large, indicating a stiff structure. During thaw, the ISM drops and at locations 3 and 7 it levels off, indicating no substantial spring thaw weakening (Fig. 9b). As indicated above, no FWD data were obtained during the most critical period from 29 March through 5 April. A similar trend was seen in the basin area (Fig. 9a). At the other locations in Figure 9b, some thaw weakening was observed. If the pavement structure is considered to have fully recovered on 23 April, the amount of thaw weakening shown by the ISM is approximately 17 to 25%. This is lower than that predicted by the basin area method.

Central Wisconsin Airport

The same observations of the increase in basin area as thaw progressed were also made at CWA (Fig. 10a,b). At some locations, we observed that the basin areas are a function of the pavement surface temperature during the recovery period (Fig. 10c). As the temperature changed, so did the basin area.

A study was made to see if there was any relationship between surface temperature and ISM or basin area. Figures 12a and 13a show that there is no relationship between either basin area or ISM with surface temperature at OCA. The data around 5°C indicate some form of relationship. However, we felt that the decrease in basin area or increase in ISM was probably attributable to the presence of frozen subsurface layers.

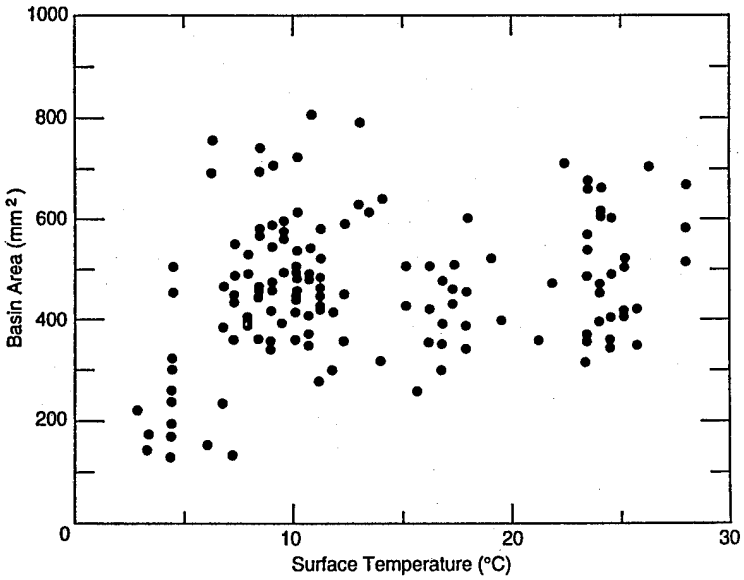

a. Outagamie County Airport.

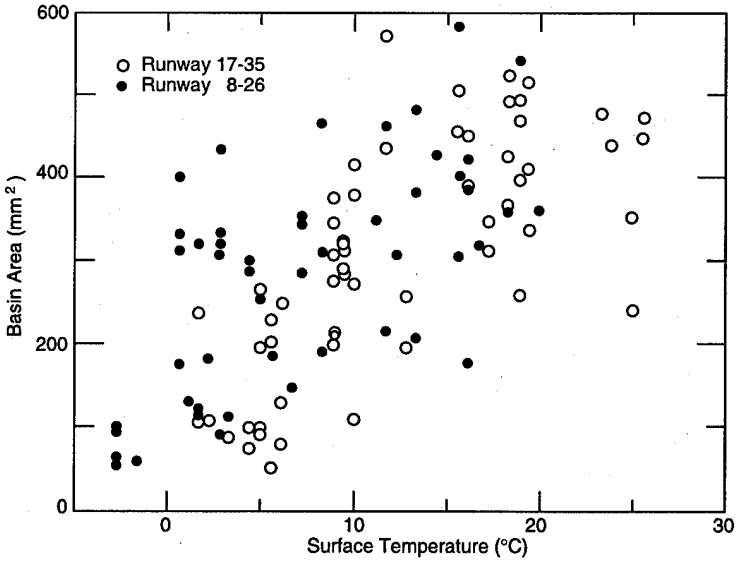

b. Central Wisconsin Airport.

Figure 12. Relationship between surface temperature and basin area.

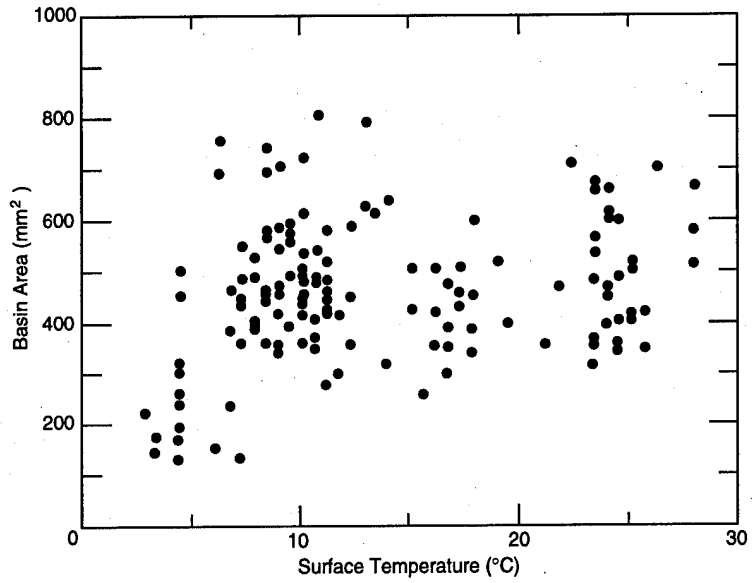

a. Outagamie County Airport.

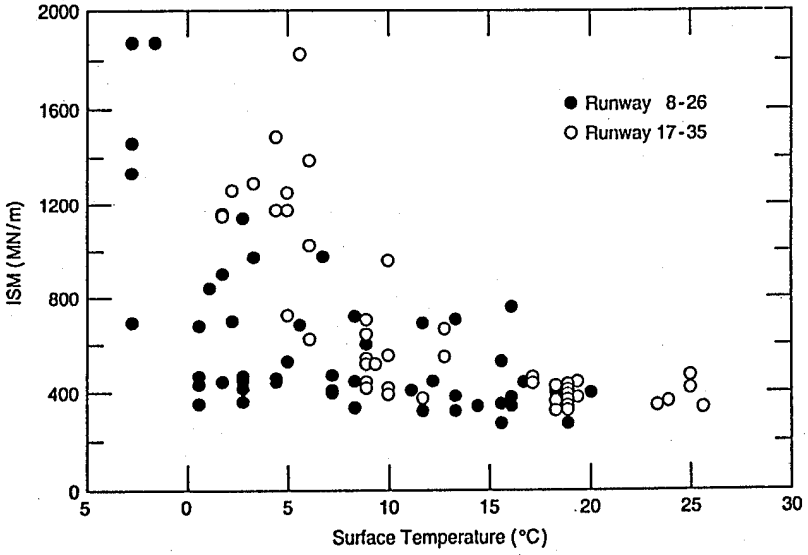

b. Central Wisconsin Airport.

Figure 13. Relationship between surface temperature and ISM.

At CWA, however, it was apparent from Figure 12b that the basin area on both runways increased with increasing surface temperature. The ISM (Fig. 13b) was fairly indifferent to surface temperatures greater than 10°C. The earlier effects could be explained by the changes in subsurface layers as thaw progressed.

Initially, we thought that the effect on the basin area was attributable to curling of the PCC pavements with temperature gradients, since the slab area on runway 17/35 was 7.6 m square and that on runway 8/26 was 6.1 by 3.8 m. However, we found that the slab dimensions at OCA were also 6.1 by 3.8 m. The big difference between OCA and CWA is the subsurface conditions. At CWA, bedrock is close to the surface in some locations. It is possible that, because of the shallow bedrock locations, the frozen and thawed layers have a greater effect on the basin area, as reflected by the surface temperature. This does not explain the change in the basin area in the recovery period, where the temperatures were above 0°C.

Backcalculation of layer moduli

Layer moduli were backcalculated using WESDEF and ILLIBACK. WESDEF was developed by the Corps of Engineers (Waterways Experiment Station). Although it is considered to be a five-layer analytical tool, it can backcalculate a maximum of four layers at one time. The fifth (bottom) layer has been "fixed" to act as a rigid layer. From our experience, reasonable results are obtained if the number of backcalculated layers is kept to three. We attempted to backcalculate the layer moduli of the PCC pavement structures at OCA and CWA. The pavement structure at OCA was idealized as shown in Figure 14a. The idealized pavement structure used at CWA is shown in Figure 14b. The depth of subgrade to bedrock at CWA was estimated from drawings found in a pavement evaluation report (CMT 1984).

In the first attempt at OCA, the moduli of all three layers during the spring thaw period were backcalculated. We found, in most cases, that errors between the calculated and measured deflections were large (more than 50%). We also found that, in many instances, the PCC modulus exceeded the upper limit of 69,000 MPa set in the program (the modulus of PCC is usually in the range of 27,000 to 42,000 MPa) and the base course modulus was near zero (in some cases it was zero). In the subsequent attempt, the PCC layer modulus was fixed at 27,580, 34,475 or 41,370 MPa. The following observations were made from the results:

1. Increasing the PCC stiffness from 27,580 to 41,370 MPa reduced the errors to more reasonable (AA <20%) differences between the measured and

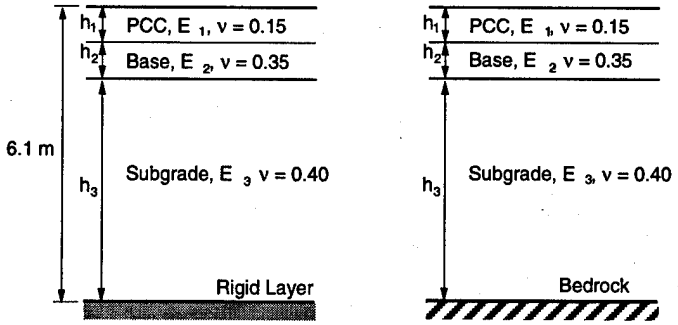

a. OCA. *b. CWA.*

Figure 14. Idealized pavement structures.

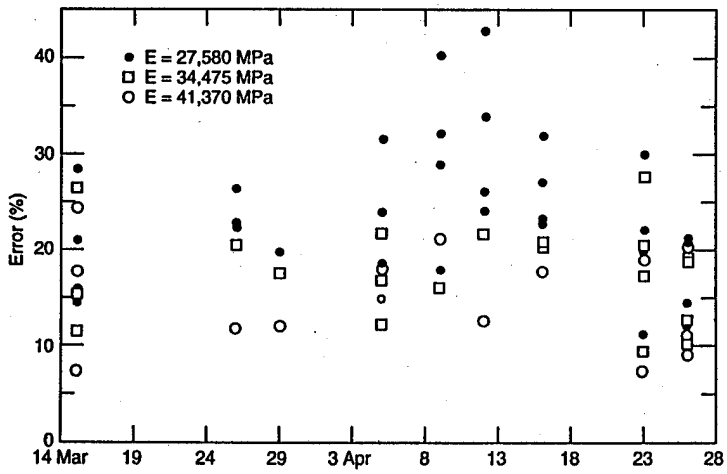

Figure 15. Effect of PCC Modulus on WESDEF absolute error (OCA).

calculated the deflections (Fig. 15). The Absolute Arithmetic (AA) error is the absolute sum of the errors between measured and calculated deflections for the seven sensors.

2. Changing the PCC modulus within the range did not significantly affect the subgrade modulus (Fig. 16). We also found that the subgrade modulus obtained from the first attempt, i.e., when the modulus of the PCC layer was not established at some particular value, was very similar to that obtained when it was. This infers that, as far as the subgrade modulus is concerned, large differences between the measured and calculated deflections can be tolerated for PCC pavement.

Changing the PCC modulus generally had a significant effect on the base course modulus. Results generated by increasing the PCC modulus showed a decrease in the backcalculated base course modulus. However, in general at OCA, the backcalculated moduli were quite low, as shown in Figure 17. With the exception of a few locations, the results were too erratic to make any meaningful conclusions.

At CWA, we selected a number of sites (FWD sites 2, 6 and 9 on runway 8/26 and 15 to 19 on runway 17/35) and attempted to backcalculate the layer modulus during the thaw period. While at OCA bedrock was at least 4 m deep, at CWA bedrock was close to the surface at some of the FWD locations. The sites selected represented bedrock at various depths. Thicknesses of the subgrade layers are shown in Table 5. We also attempted to backcalculate the base course modulus under FWD location 3. Location 3 was different from the other sites because the base course layer was founded directly on top of the bedrock. The structure at FWD location 3 was 330 mm of PCC over 1220 mm of base over bedrock. We were unable to get reasonable agreement between the calculated and mea-

Table 5. Thickness of subgrade at backcalculated FWD locations.

FWD location	*Subgrade thickness (mm)*	*FWD location*	*Subgrade thickness (mm)*
2	2435	16	1829
6	1092	17	3785
9	5613	18	3073
15	610	19	2743

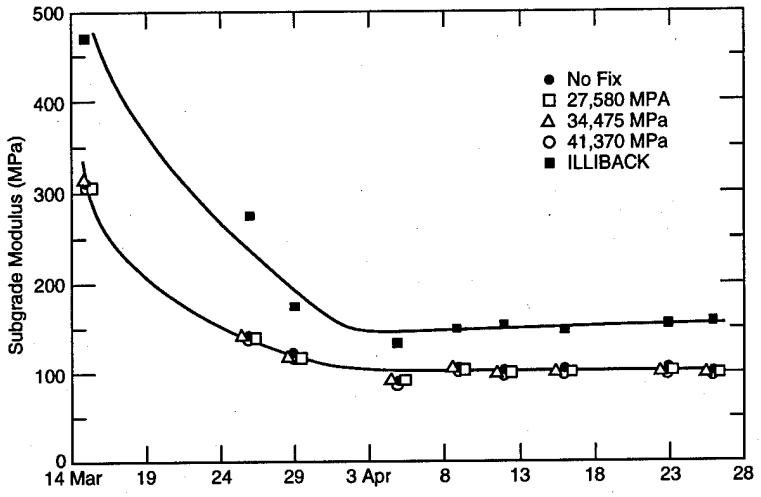

a. FWD location 3.

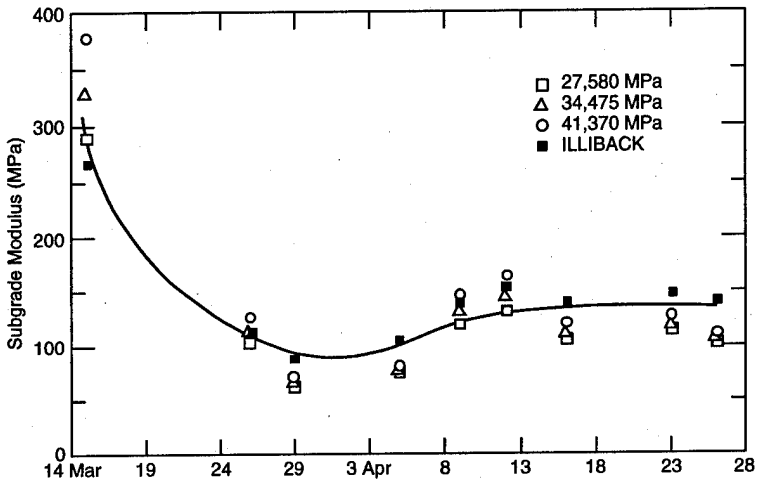

b. FWD location 9.

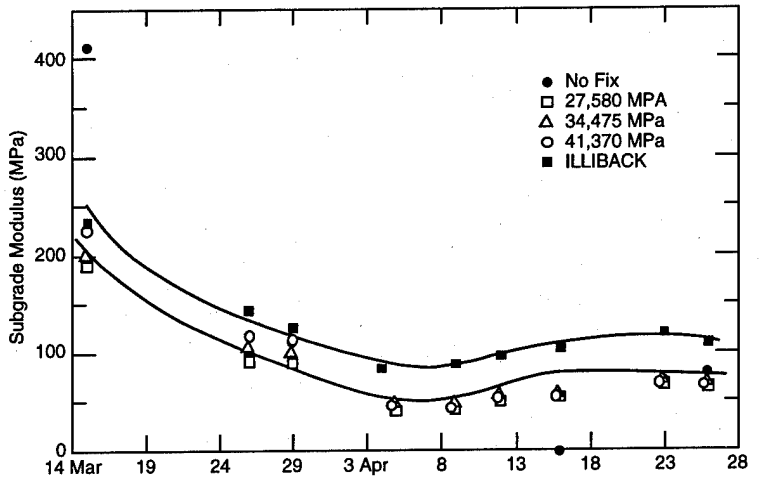

c. FWD location 22.

Figure 16. Effect of PCC modulus on change in subgrade modulus from WESDEF during spring thaw at Outagamie County Airport. Comparison of subgrade modulus from ILLIBACK and WESDEF.

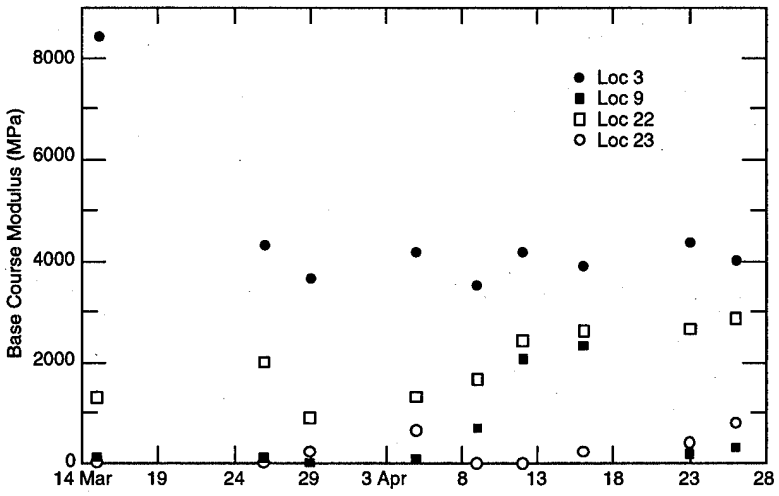

Figure 17. Backcalculated base course modulus using WESDEF (OCA).

sured deflections. The AA error was in the vicinity of 450%.

Solutions could not be obtained for locations 6, 15 and 16. In many cases, WESDEF printed a "THIS MATRIX HAS NO SOLUTION" message. At other times, the backcalculated base course modulus was zero, or very close to zero. It is interesting to note that at these locations the bedrock was quite close to the surface (less than 2 m). At the other locations, with a few exceptional days, the error between the calculated and measured values was acceptable (Table 6). The lack of values in the base modulus, subgrade modulus and error columns in Table 6 indicate that either it was not possible to converge to a solution or that the base course modulus was extremely low (less than 1 MPa). When only the AA error column lacks values, it means that we used the backcalculated results from WESDEF but ignored the controlling layer modulus range, i.e., the backcalculated modulus was either above or below the prescribed range.

The effect of changing the PCC modulus is shown in Table 7 for FWD locations 9, 17, 18 and 19. As

Table 6. Backcalculated modulus at CWA using WESDEF.

Date	*FWD location*	*PCC (MPa)*	*Base (MPa)*	*Subgrade (MPa)*	*AA Error (%)*	*Date*	*FWD location*	*PCC (MPa)*	*Base (MPa)*	*Subgrade (MPa)*	*AA Error (%)*
20 Mar	2	27,580	54,148	433	—	10 Apr	17	27,580	1,520	58	8.4
24 Mar	2	27,580	6,807	214	26.7	14 Apr	17	27,580	3,717	133	3.9
27 Mar	2	27,580	5,096	97	12.0	17 Apr	17	27,580	2,416	57	8.7
4 Apr	2	27,580	2,123	70	12.3	21 Apr	17	27,580	3,560	50	8.9
7 Apr	2	27,580	1,832	56	17.1	24 Apr	17	27,580	18,212	18	129.2
10 Apr	2	27,580	2,002	70	16.0	18 Mar	18	27,580	149	595	—
14 Apr	2	27,580	2,791	65	21.4	24 Mar	18	27,580	3,216	367	23.0
17 Apr	2	27,580	2,284	56	16.9	27 Mar	18	27,580	3,645	32	10.8
21 Apr	2	27,580	4,087	56	15.0	4 Apr	18	27,580	4,027	39	9.6
24 Apr	2	27,580	2,402	47	16.3	7 Apr	18	27,580	3,499	26	4.6
20 Mar	9	27,580	4,965	825	13.3	10 Apr	18	27,580	4,713	29	9.1
24 Mar	9	27,580	1,935	455	17.4	14 Apr	18	27,580	2,611	82	5.2
27 Mar	9	27,580	1,373	162	20.6	17 Apr	18	27,580	2,035	39	7.0
4 Apr	9	27,580	643	139	14.5	21 Apr	18	27,580	—	—	—
7 Apr	9	27,580	526	62	14.4	24 Apr	18	27,580	2,572	35	8.9
10 Apr	9	27,580	1,050	107	16.9	18 Mar	19	27,580	5,648	272	11.4
14 Apr	9	27,580	1,495	111	9.5	24 Mar	19	27,580	5,133	316	—
17 Apr	9	27,580	1,200	81	13.8	27 Mar	19	27,580	—	—	—
21 Apr	9	27,580	1,547	116	16.9	4 Apr	19	27,580	—	—	—
24 Apr	9	27,580	1,612	99	18.3	7 Apr	19	27,580	2,163	29	8.2
18 Mar	17	27,580	5,956	425	31.6	10 Apr	19	27,580	1,852	32	7.0
24 Mar	17	27,580	4,802	589	12.8	14 Apr	19	27,580	—	—	—
27 Mar	17	27,580	2,071	157	11.6	17 Apr	19	27,580	1,482	29	9.3
4 Apr	17	27,580	2,821	131	5.9	21 Apr	19	27,580	—	—	—
7 Apr	17	27,580	1,747	51	10.9	24 Apr	19	27,580	1,891	30	8.8

Table 7. Effect of change in PCC modulus on base and subgrade modulus.

Date	FWD location	PCC (MPa)	Base (MPa)	Subgrade (MPa)	AA error (%)	PCC (MPa)	Base (MPa)	Subgrade (MPa)	AA error (%)
20 Mar	9	27,580	4,965	825	13.3	34,475	3617	828	12.3
24 Mar	9	27,580	1,935	455	17.4	34,475	1045	463	12.8
27 Mar	9	27,580	1,373	162	20.6	34,475	529	165	17.7
4 Apr	9	27,580	643	139	14.5	34,475	81	155	10.3
7 Apr	9	27,580	526	62	14.4	34,475	16	81	11.5
10 Apr	9	27,580	1,050	107	16.9	34,475	255	110	14.3
14 Apr	9	27,580	1,495	111	9.5	34,475	537	113	8.9
17 Apr	9	27,580	1,200	81	13.8	34,475	387	82	11.7
21 Apr	9	27,580	1,547	116	16.9	34,475	685	118	15.1
24 Apr	9	27,580	1,612	99	18.3	34,475	749	100	16.2
18 Mar	17	27,580	5,956	425	31.6	34,475	4092	429	32.2
24 Mar	17	27,580	4,802	589	12.8	34,475	3038	595	9.7
27 Mar	17	27,580	2,071	157	11.6	34,475	—	—	—
4 Apr	17	27,580	2,821	131	5.9	34,475	1455	134	5.8
7 Apr	17	27,580	1,747	51	10.9	34,475	639	52	9.4
10 Apr	17	27,580	1,520	58	8.4	34,475	316	59	8.3
14 Apr	17	27,580	3,717	133	3.9	34,475	2282	135	4.2
17 Apr	17	27,580	2,416	57	8.7	34,475	—	—	—
21 Apr	17	27,580	3,560	50	8.9	34,475	2350	49	7.8
24 Apr	17	27,580	18,212	18	129.2	34,475	—	—	—
18 Mar	18	27,580	149	595	—	34,475	—	—	—
24 Mar	18	27,580	3,216	367	23.0	34,475	1750	373	19.4
27 Mar	18	27,580	3,645	32	10.8	34,475	2335	33	9.2
4 Apr	18	27,580	4,027	39	9.6	34,475	—	—	—
7 Apr	18	27,580	3,499	26	4.6	34,475	2241	26	3.5
10 Apr	18	27,580	4,713	29	9.1	34,475	2609	30	2.1
14 Apr	18	27,580	2,611	82	5.2	34,475	—	—	—
17 Apr	18	27,580	2,035	39	7.0	34,475	708	40	7.2
21 Apr	18	27,580	—	—	—	34,475	—	—	—
24 Apr	18	27,580	2,572	35	8.9	34,475	1473	36	9.7
18 Mar	19	27,580	5,648	272	11.4	34,475	3839	278	8.6
24 Mar	19	27,580	5,133	316	—	34,475	3195	319	11.5
27 Mar	19	27,580	—	—	—	34,475	—	—	—
4 Apr	19	27,580	—	—	—	34,475	—	—	—
7 Apr	19	27,580	2,163	29	8.2	34,475	830	30	8.0
10 Apr	19	27,580	1,852	32	7.0	34,475	551	33	7.4
14 Apr	19	27,580	—	—	—	34,475	—	—	—
17 Apr	19	27,580	1,482	29	9.3	34,475	444	30	8.2
21 Apr	19	27,580	—	—	—	34,475	—	—	—
24 Apr	19	27,580	1,891	30	8.8	34,475	591	31	8.3

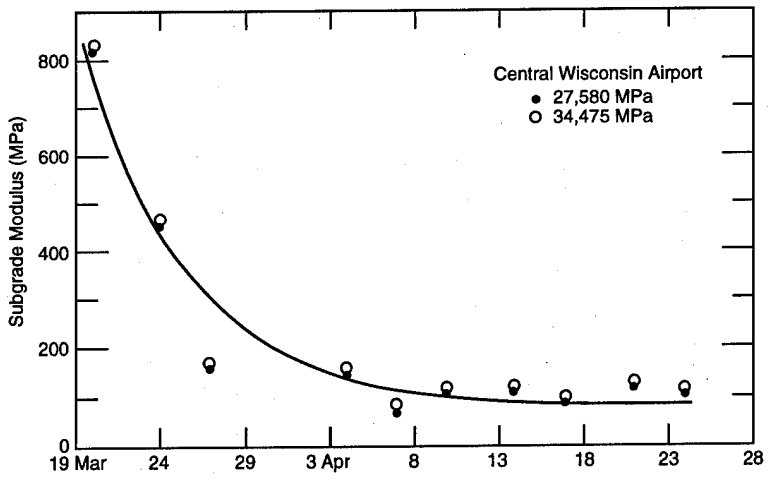

Figure 18. Change in subgrade modulus during spring thaw (FWD location 9, CWA).

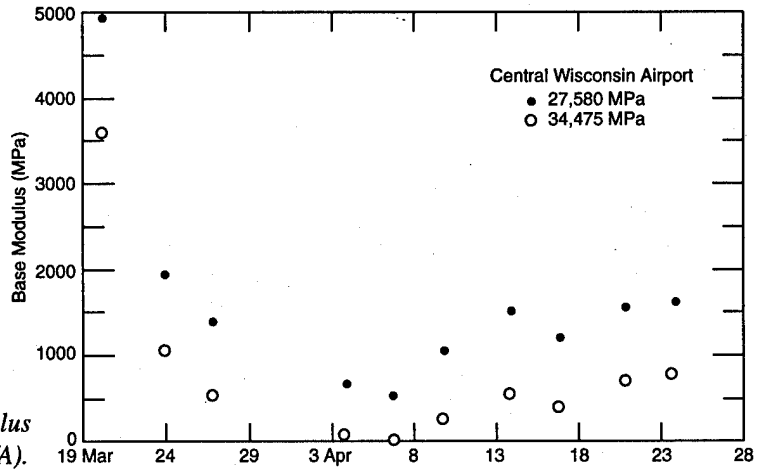

Figure 19. Change in base course modulus during spring thaw (FWD location 9, CWA).

found at OCA, changing the PCC modulus did not significantly affect the backcalculated subgrade modulus (Fig. 18 for location 9). However, as was also found at OCA, changing the PCC modulus had a significant effect on the base course modulus (Fig. 19). Trends in the data indicate that the base was in a weakened state from the end of March through about mid-April. The values reported here for the base course modulus are still considered too large. By combining the change in the PCC modulus with changing the different layer thicknesses, singularly or simultaneously, we found that, in some cases, we were able to reduce the base course modulus to more reasonable values. However, we felt that changing the layer thicknesses was introducing another unknown variable into the analysis. Therefore, although the base course moduli are high, we have opted to present the results obtained for the reported thicknesses. It is very clear that a small coring program should be conducted with FWD testing to verify thicknesses. Irwin et al. (1989) reported that a 6-mm change in layer thickness has a large impact on the backcalculated layer modulus. Also note that, although changing the PCC modulus affected the base course modulus, the change produced very small changes in the absolute error (Table 7).

ILLIBACK was also used to backcalculate the layer moduli. This procedure was developed by Ioannides et al. (1989) as a closed form of backcalculation for a two-layer rigid pavement system using principles of dimensional analysis. For a given deflection sensor distribution, they found a unique relationship between the FWD deflection basin area and the radius of relative stiffness of the pavement subgrade system (l). They then developed relationships between the ratios of nondimensional deflections and actual FWD deflections and l for a constant FWD loading plate radius (300 mm). These relationships were used with the applied load to calculate the coefficient of subgrade reaction (k), PCC modulus (E_c) and subgrade modulus (E_s).

The elastic modulus of concrete (E_c), elastic subgrade modulus (E_s) and the coefficient of subgrade reaction (k) can be determined from

$$E_c = \frac{12(1-\mu^2)}{h^3} \times \frac{d_i}{D_i} \times Pl^2$$

$$E_s = (1-\nu^2) \times \frac{d_i}{D_i} \times \frac{2P}{l}$$

$$k = \frac{d_i}{D_i} \times \frac{2P}{l}$$

where μ = Poisson's ratio for concrete
ν = Poisson's ratio for subgrade
P = applied FWD load
D_i = FWD deflection measurement at sensor i
d_i = nondimensional deflection at sensor i
h = PCC layer thickness.

Additional information on this method can be found in Ioannides et al. (1989) and Barenberg and Ioannides (1989). Barenberg and Ioannides have developed figures to determine l from the deflection basin area; l is then used to determine d_i. The base and subgrade were modeled as a single composite structure at OCA. At CWA, the base, subgrade and bedrock were combined into a single layer.

Typical changes in the 'subgrade' modulus during spring thaw at OCA are shown in Figure 16. The 'subgrade' modulus backcalculated from ILLIBACK was approximately 25% larger than that from WESDEF, as shown in Figure 20. The backcalculated PCC modulus for some of the FWD sites is shown in Figure 21. These are typical results and are also representative of other sites at OCA. They are also within the range of reported values, varying between 21,000 to 42,000 MPa. The data also indicate that the PCC modulus increased by about 15% over the duration of the monitored period.

Based on the results, relationships between the subgrade modulus and the basin area or ISM were devel-

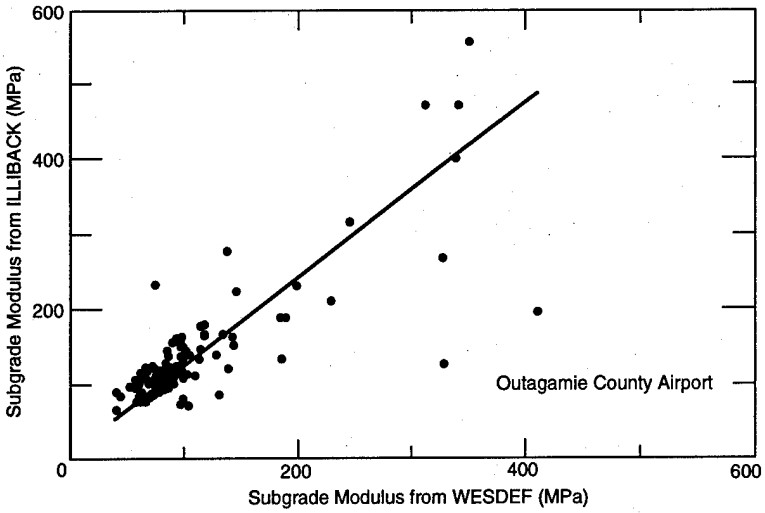

Figure 20. Relationship between subgrade moduli backcalculated by WESDEF and ILLIBACK.

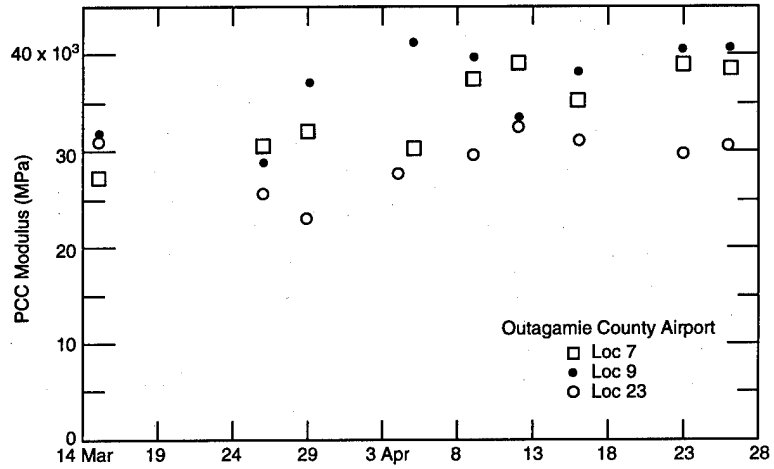

Figure 21. Typical backcalculated PCC modulus from ILLIBACK (OCA).

oped. Basin area results from ILLIBACK and WESDEF are shown for both OCA and CWA in Figures 22 and 23. In Figure 22, the total basin area was calculated using all seven deflections. In Figure 23, the basin area was calculated using the third to seventh deflections.

Previously, we had determined that the thaw depth under AC pavements could be related to the partial basin area calculated using the third to seventh deflections (Janoo and Berg 1990). The current data indicate that this partial basin area ($A_{3\text{-}7}$) may be related to the subgrade modulus. The figures show that as the total basin area or partial basin area increased, the subgrade modulus decreased. A power relationship was found to best fit the total basin area or partial basin area and the subgrade modulus. We also found that a better correlation existed with the subgrade modulus obtained from ILLIBACK. The use of the partial basin area ($A_{3\text{-}7}$) (Fig. 23) did not significantly increase the correlation at OCA. We used other combinations of deflections to calculate the partial basin areas and found that none significantly increased the correlation with the calculated subgrade modulus.

A similar relationship between ISM and subgrade modulus is shown in Figure 24. A second-order polynomial function provides the best fit to the data. Again, a better correlation is obtained using the results from ILLIBACK.

The results from OCA and CWA are combined in Figures 25 and 26. In Figure 25a presents a relationship developed between the measured total basin area and subgrade modulus calculated from ILLIBACK for both sites. An excellent correlation between total basin area and subgrade modulus is found. In Figure 25b, the relationship developed between the total basin area and subgrade modulus calculated from WESDEF for both sites is presented. There are two distinct trends. This is probably attributable to the separation of the base and subgrade in WESDEF. Again, a power curve seems to

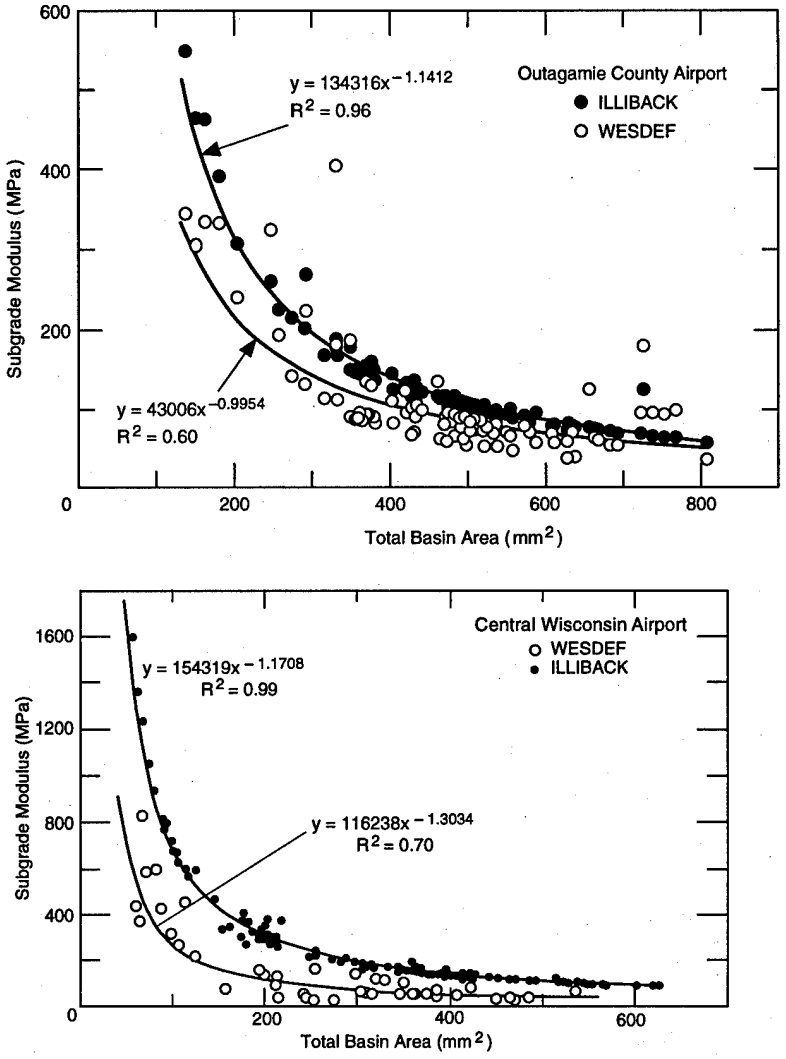

Figure 22. Relationship between measured total basin area and calculated subgrade modulus.

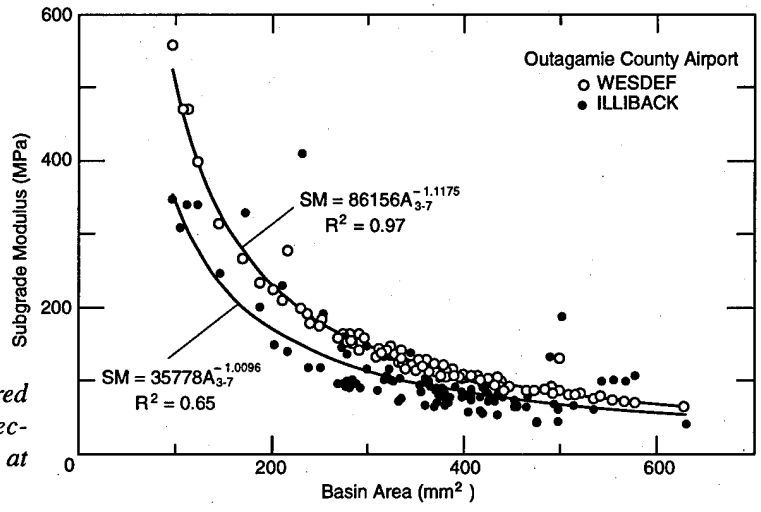

Figure 23. Relationship between measured partial basin area (third–seventh deflections) and calculated subgrade modulus at Outagamie County Airport.

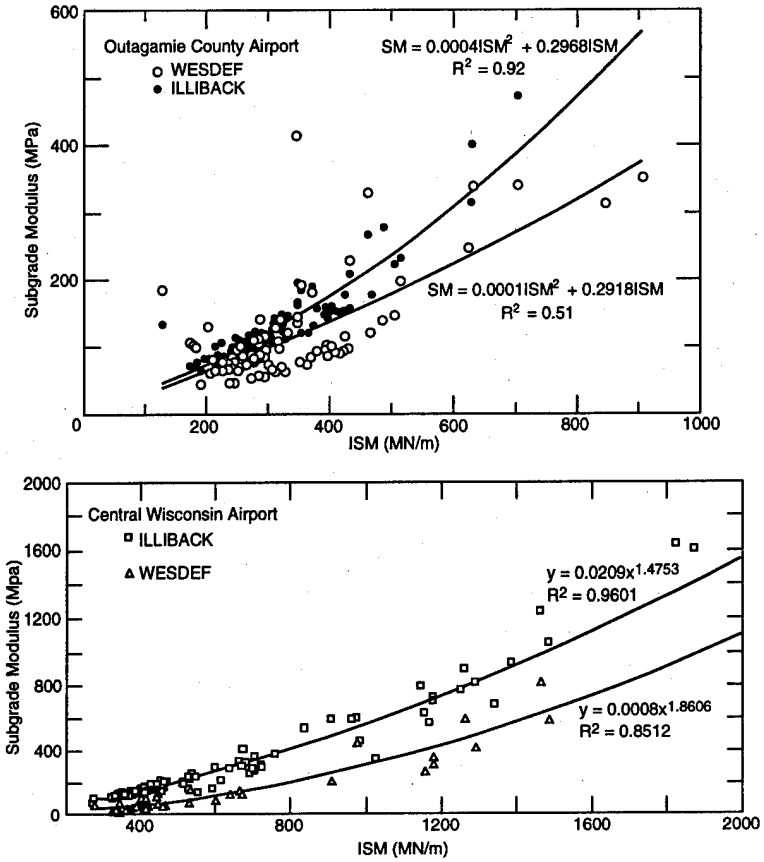

Figure 24. Relationship between measured ISM and calculated subgrade modulus at Outagamie County Airport and Central Wisconsin Airport.

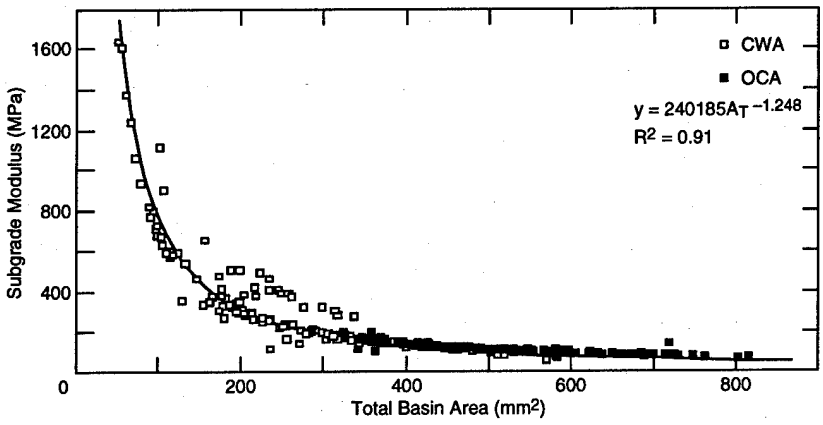

a. Calculated using ILLIBACK.

Figure 25. Relationship between total basin area and subgrade modulus at Outagamie County Airport and Central Wisconsin Airport.

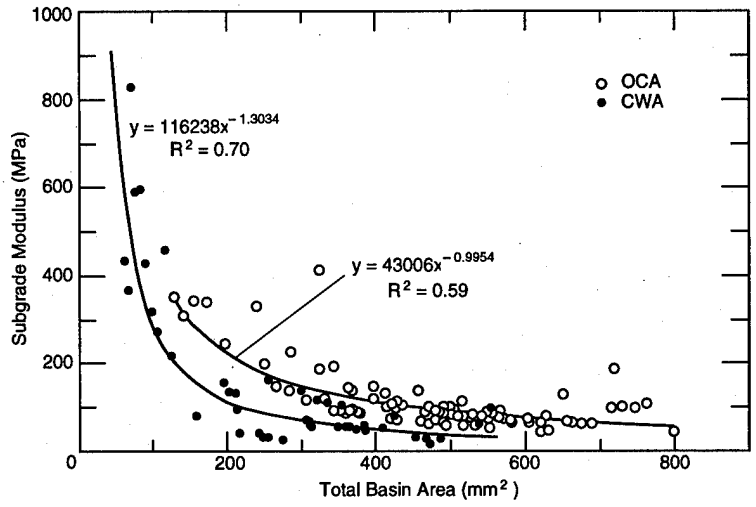

b. Calculated using WESDEF.

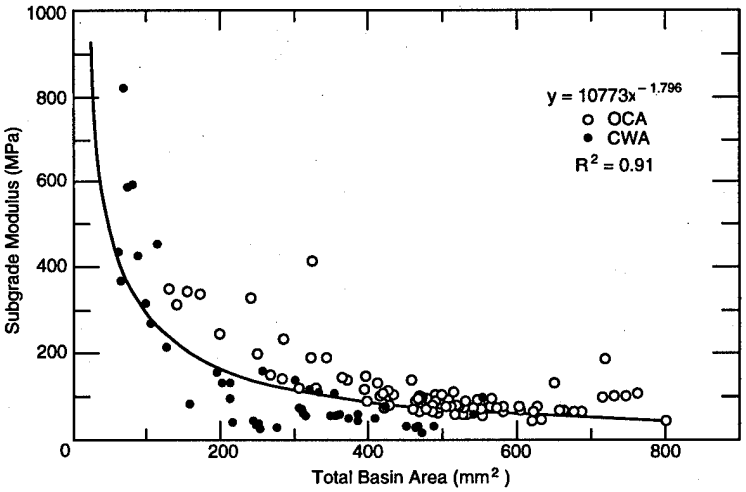

c. Calculated using WESDEF with a single power trend.

Figure 25 (cont'd).

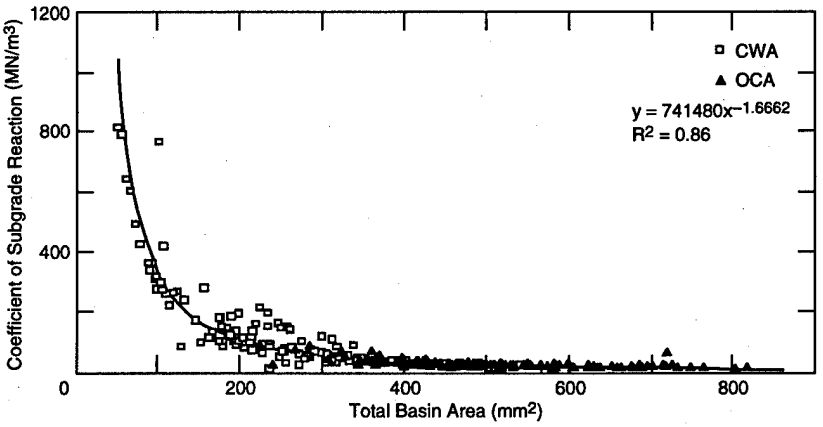

Figure 26. Relationship between total basin area and coefficient of subgrade reaction calculated using ILLIBACK at Outagamie County Airport and Central Wisconsin Airport.

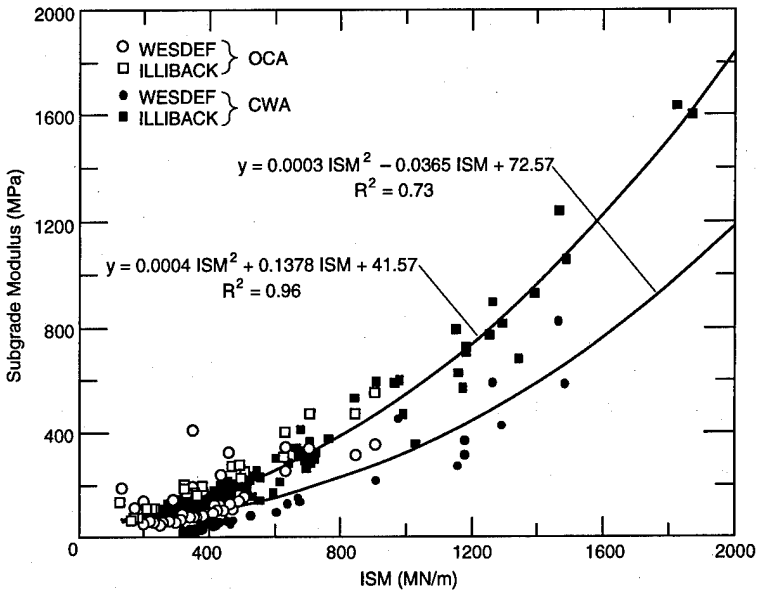

Figure 27. Relationship between ISM and subgrade modulus at OCA and CWA.

best fit the data, so for estimation, a single power trend was applied to the data as shown in Figure 25c. Figure 26 shows the relationship between the measured total basin area and the coefficient of subgrade reaction (k) computed from ILLIBACK for both sites The following equations have been developed from the ILLIBACK results and can be used to estimate the subgrade modulus and the coefficient of subgrade reaction (k)

$$SM = 240{,}185 A_T^{-1.248} \qquad (R^2 = 0.91)$$

$$k = 741{,}480 A_T^{-1.6662} \qquad (R^2 = 0.86)$$

where SM = subgrade modulus (MPa)
A_T = total basin area (mm^2)
k = coefficient of subgrade reaction (MN/m^3).

In Figure 27, the relationship of ISM and subgrade modulus for both OCA and CWA is shown. Again, a single power curve can be fitted to the data.

Current criteria for PCC pavements state that failure occurs when the horizontal tensile stress at the bottom of the PCC layer is equal to or greater than the flexural strength of the slab. The flexural strength reported at OCA and CWA was 4.5 MPa. The two types of aircraft used for these simulations were the MD-DC9 and the Boeing 757. The gear loads, tire spacings and radii were obtained from the FAALEA computer program and are presented in Tables 8 and 9.

Several FWD locations were selected from each airport for computing the tensile stress at the bottom of the PCC layer on different days during the monitoring period. The damage (D) reported here is defined as the ratio of maximum horizontal (tensile) stress to the flexural

Table 8. Gear loading for the MD-DC9 and Boeing 757.

Aircraft type	*Design load (MN)*	*% of design load on each main gear*	*Load on main gear (MN)*
MD-DC9	480	47.5	228.2
Boeing 757	1112	47.5	528.2

Table 9. Gear information for computer simulations of the MD-DC9 and Boeing 757.

Aircraft type	*Tire no.*	*Radius (mm)*	*Contact area (m²)*	*Contact pressure (kPa)*	*Load on tire (kN)*	*X-cord (mm)*	*Y-cord (mm)*
MD-DC9	1	181.4	0.103	1103	114.1	–330.2	0
	2	181.4	0.103	1103	114.1	330.2	0
Boeing 757	1	189.5	0.113	1172	132.1	–431.8	0
	2	189.5	0.113	1172	132.1	431.8	0
	3	189.5	0.113	1172	132.1	–431.8	1143
	4	189.5	0.113	1172	132.1	431.8	1143

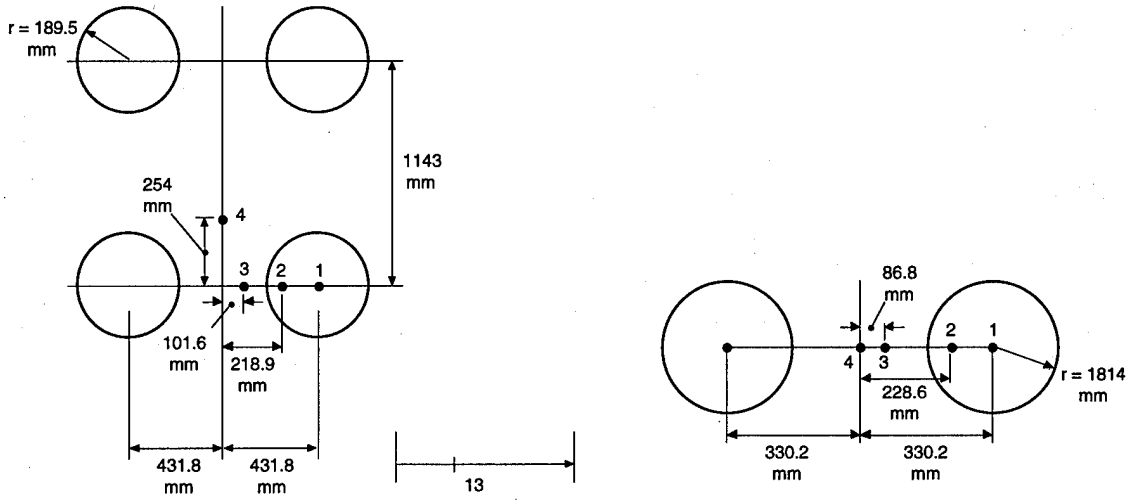

Figure 28. Configuration and location of stress calculations for Boeing 757 and MD-DC9.

strength of the PCC layer

$$D = \frac{\sigma_{tensile}}{\sigma_{flexural}}.$$

Layer moduli from ILLIBACK were used to represent the pavement structures. The computer program BISAR was used to calculate the stresses at locations shown in Figure 28. The stress calculation points are the same as those used in FAALEA. The results are tabulated in Table 10 and damage is shown for CWA in Figure 29. As thaw progresses, the amount of damage increases until thawing is complete; then it levels off with time. The results also indicate that the damage is a function of pavement thickness, a linear relationship being found in the 24 April data from CWA (Fig. 30).

The thinner pavements (178 to 203 mm) at OCA showed potential near-failure conditions during the spring thaw (Fig. 31). Some pavements recovered somewhat, as typified by location 9 (Fig. 31). The thicker section (location 23, 254 mm) had a similar amount of damage as those sections of similar thickness at CWA; however, the OCA sections did not exhibit the loss during the thawing period observed at CWA.

The horizontal stresses are plotted as functions of the subgrade modulus, coefficient of subgrade reaction and the PCC modulus in Figures 32–34. With respect to the PCC modulus, no trends were seen (Fig. 34), and nonlinear trends were observed for all of

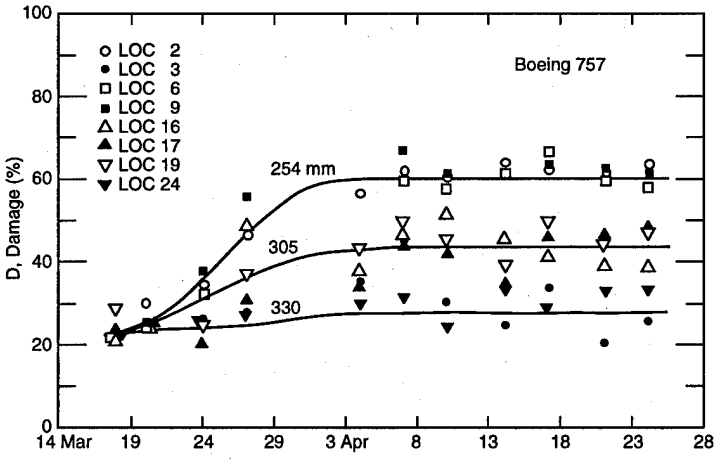

Figure 29. Amount of damage during spring thaw at Central Wisconsin Airport.

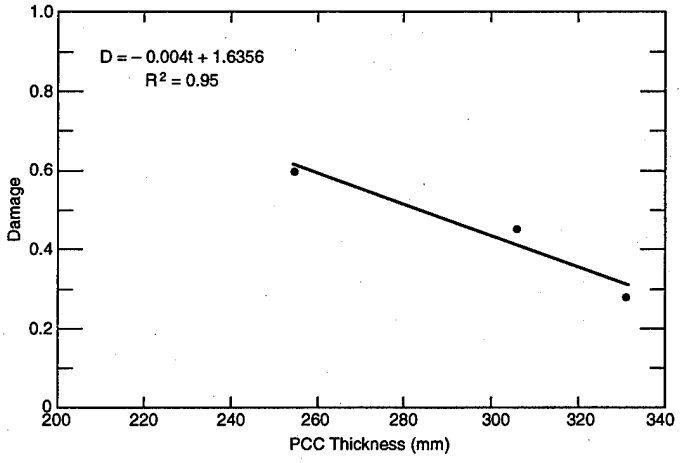

Figure 30. Effect of pavement thickness on damage at Central Wisconsin Airport.

Table 10. Ratio of maximum horizontal tensile stress to flexural strength during spring thaw.

Date	FWD location	Damage ratio Boeing757	Damage ratio MD DC9
a. Central Wisconsin Airport			
20 Mar	2	0.29	0.32
24 Mar	2	0.34	0.38
27 Mar	2	0.46	0.50
4 Apr	2	0.56	0.58
7 Apr	2	0.62	0.62
10 Apr	2	0.60	0.61
14 Apr	2	0.64	0.63
17 Apr	2	0.62	0.62
21 Apr	2	0.62	0.62
24 Apr	2	0.63	0.63
20 Mar	3	0.25	0.27
24 Mar	3	0.26	0.28
27 Mar	3	0.27	0.29
4 Apr	3	0.35	0.35
7 Apr	3	0.45	0.42
10 Apr	3	0.30	0.32
14 Apr	3	0.25	0.27
17 Apr	3	0.33	0.34
21 Apr	3	0.20	0.22
24 Apr	3	0.25	0.27
20 Mar	6	0.25	0.26
24 Mar	6	0.32	0.35
27 Mar	6	0.49	0.52
4 Apr	6	0.50	0.53
7 Apr	6	0.60	0.60
10 Apr	6	0.58	0.59
14 Apr	6	0.63	0.62
17 Apr	6	0.66	0.65
21 Apr	6	0.61	0.61
24 Apr	6	0.58	0.59
20 Mar	9	0.25	0.27
24 Mar	9	0.38	0.41
27 Mar	9	0.55	0.57
4 Apr	9	0.53	0.55
7 Apr	9	0.67	0.65
10 Apr	9	0.61	0.61
14 Apr	9	0.55	0.57
17 Apr	9	0.63	0.63
21 Apr	9	0.62	0.62
24 Apr	9	0.61	0.61
18 Mar	16	0.22	0.24
24 Mar	16	0.24	0.26
27 Mar	16	0.48	0.46
4 Apr	16	0.37	0.39
7 Apr	16	0.46	0.45
10 Apr	16	0.51	0.48
14 Apr	16	0.46	0.45
17 Apr	16	0.41	0.42
21 Apr	16	0.39	0.40
24 Apr	16	0.39	0.40
18 Mar	17	0.23	0.26
24 Mar	17	0.20	0.22
27 Mar	17	0.30	0.33
4 Apr	17	0.34	0.37
7 Apr	17	0.46	0.45
10 Apr	17	0.42	0.42
14 Apr	17	0.34	0.36
17 Apr	17	0.46	0.45
21 Apr	17	0.46	0.45
24 Apr	17	0.48	0.46
24 Mar	19	0.24	0.26
27 Mar	19	0.36	0.38
4 Apr	19	0.42	0.42
7 Apr	19	0.48	0.46
10 Apr	19	0.45	0.44
14 Apr	19	0.39	0.40
17 Apr	19	0.49	0.47
21 Apr	19	0.44	0.43
24 Apr	19	0.47	0.45
b. Outagamie County Airport			
15 Mar	1	0.52	0.55
26 Mar	1	0.59	0.60
29 Mar	1	0.56	0.57
5 Apr	1	0.00	0.61
9 Apr	1	0.64	0.63
12 Apr	1	0.58	0.59
16 Apr	1	0.63	0.63
23 Apr	1	0.48	0.51
26 Apr	1	0.61	0.61
15 Mar	4	0.55	0.60
26 Mar	4	0.78	0.83
29 Mar	4	0.92	0.94
5 Apr	4	—	1.00
9 Apr	4	0.99	0.98
12 Apr	4	0.97	0.97
16 Apr	4	1.00	0.99
23 Apr	4	0.97	0.97
26 Apr	4	0.94	—
15 Mar	9	0.64	0.70
26-Mar	9	0.81	0.86
29 Mar	9	0.97	0.97
5 Apr	9	0.95	0.95
9 Apr	9	0.85	0.88
12 Apr	9	0.78	0.83
16 Apr	9	0.84	0.87
23 Apr	9	0.84	0.87
26 Apr	9	0.85	0.88
15 Mar	23	0.79	0.87
26 Mar	23	0.80	0.88
29 Mar	23	0.91	0.99
4 Apr	23	0.96	1.04
9 Apr	23	0.99	1.06
12 Apr	23	1.00	1.07
16 Apr	23	0.97	1.04
23 Apr	23	0.90	0.97
26 Apr	23	0.96	1.03

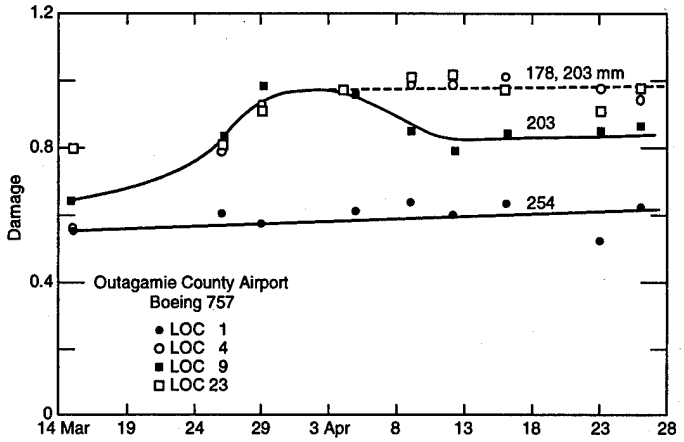

Figure 31. Amount of damage during spring thaw at Outagamie County Airport.

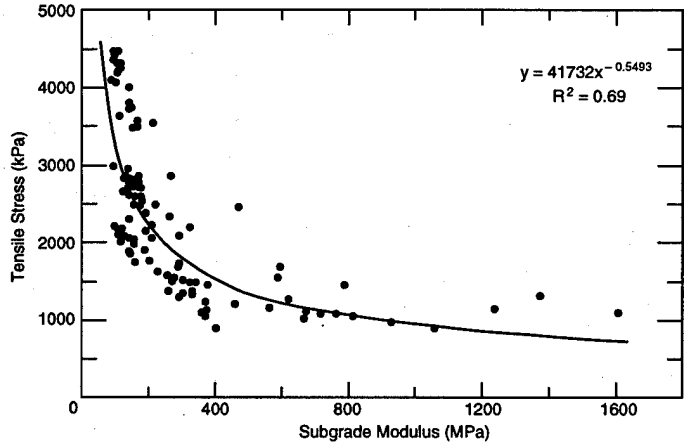

a. Boeing 757.

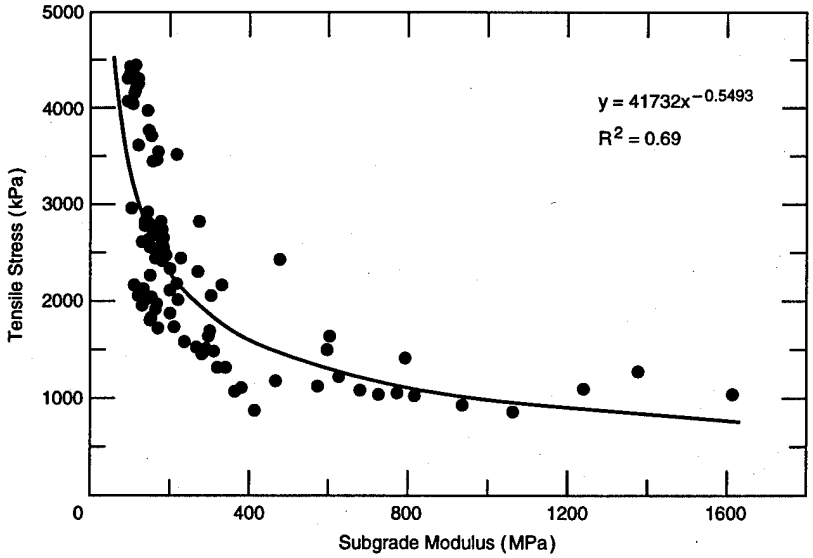

b. MD-DC9.

Figure 32. Effect of subgrade modulus on the horizontal tensile stress at the bottom of the PCC layer (OCA and CWA).

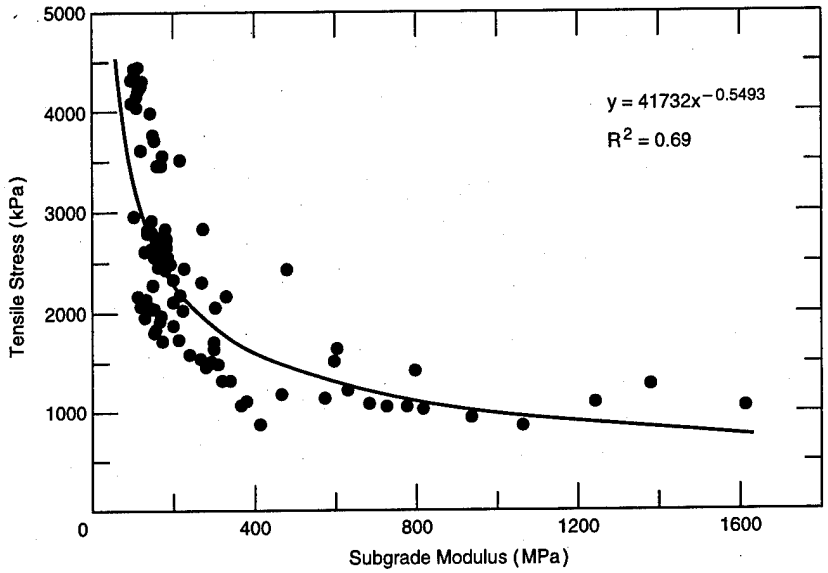

a. Boeing 757.

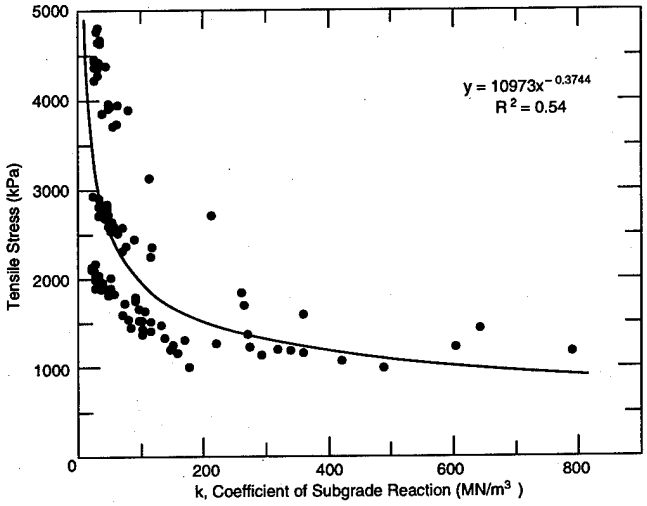

b. MD-DC9.

Figure 33. Effect of the coefficient of subgrade reaction, k, *on the horizontal tensile stress at the bottom of the PCC layer.*

the other relationships. Small differences were obtained for the Boeing 757 and the MD-DC9.

The following equation could be used to estimate the horizontal stress σ_h as a function of the subgrade modulus E_s (MPa) during the spring thaw

$$\sigma_h = 41,732\, E_s^{-0.549}.$$

We observed a similar trend between the horizontal strain and the coefficient of subgrade reaction. The following equation could be used to estimate the horizontal stress (σ_h) as a function of the coefficient of subgrade reaction, k (MN/m^3) during the spring thaw

$$\sigma_h = 12,436\, k^{-0.411}.$$

Since we found damage to be a function of thickness, σ_h was developed as a function of E_s or k and the coefficient of thickness. We found that the correlations increased when thickness was taken into consideration.

$$\sigma_h = 7360 - 1.5E_s - 17t$$

or

$$\sigma_h = 7389 - 13.02k - 17.5t$$

where t is PCC thickness (mm).

The relationship between the total basin area and the horizontal stresses (σ_h) at the bottom of the PCC layer is shown in Figure 35. A linear trend was applied to the

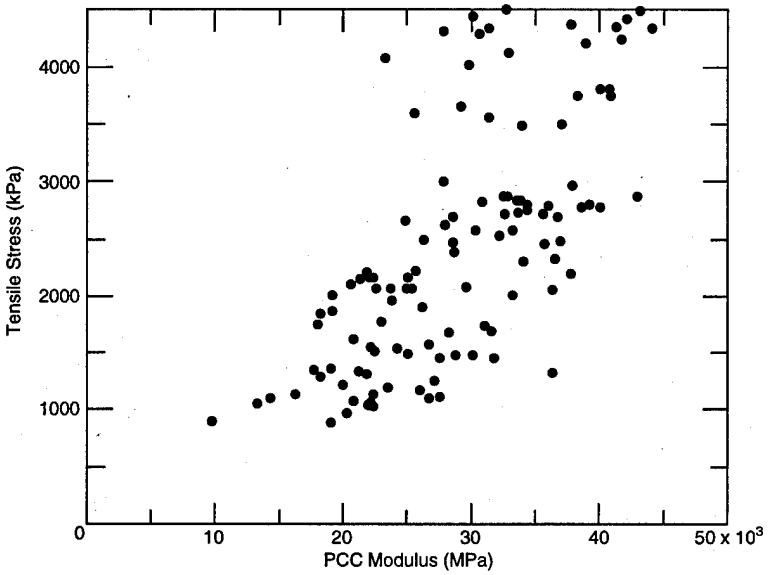

a. Boeing 757.

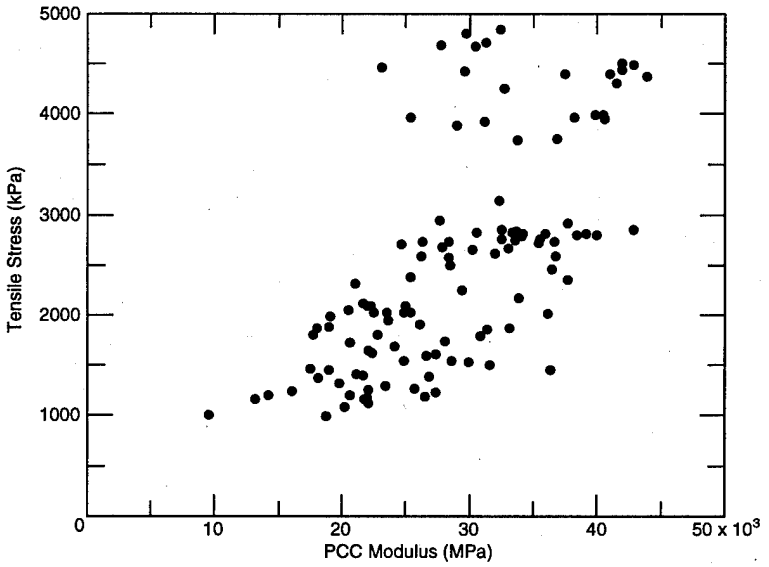

b. MD-DC9.

Figure 34. Effect of PCC modulus on the horizontal tensile stress at the bottom of the PCC layer.

results. We used partial basin areas, but found no better correlation. The following equation can be used to determine σ_h from the total basin area

$$\sigma_h = 7.35 \times A_T \qquad R^2 = 0.7.$$

The ISM can also be used to estimate σ_h, as shown in Figure 36. A power relationship was found to best describe the relationship between ISM and (σ_h)

$$\sigma_h = 357{,}068 \times ISM^{-0.8165} \qquad R^2 = 0.81.$$

LOAD TRANSFER EFFICIENCY (LTE)

Joints are generally weak points in jointed concrete pavements. Although the load transfer across joints has a great effect on the stress at the bottom of the slab, and therefore on the performance of the pavement, it is largely ignored in most evaluation schemes because of the difficulty of measuring these stresses (Foxworthy 1985). The load transfer can be inferred from the amount of deflection on both sides of the joint when a load is applied on one side of the joint. The FWD, simulating a wheel load on one side of a joint, can be used

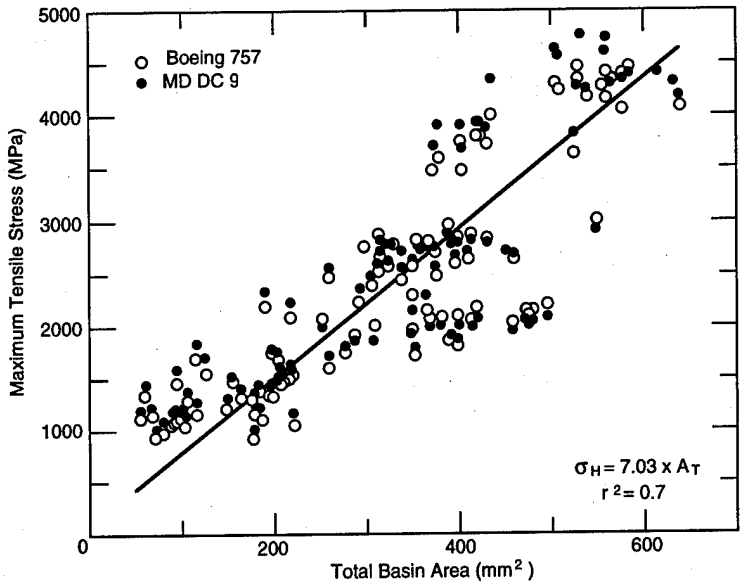

Figure 35. Linear relationship between total basin area and maximum horizontal tensile stress at bottom of PCC Layer.

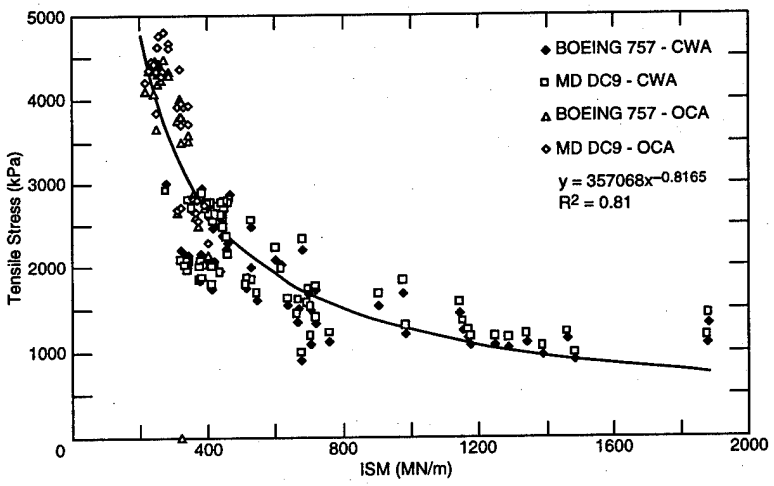

Figure 36. Relationship between ISM and horizontal tensile stress at bottom of PCC Layer.

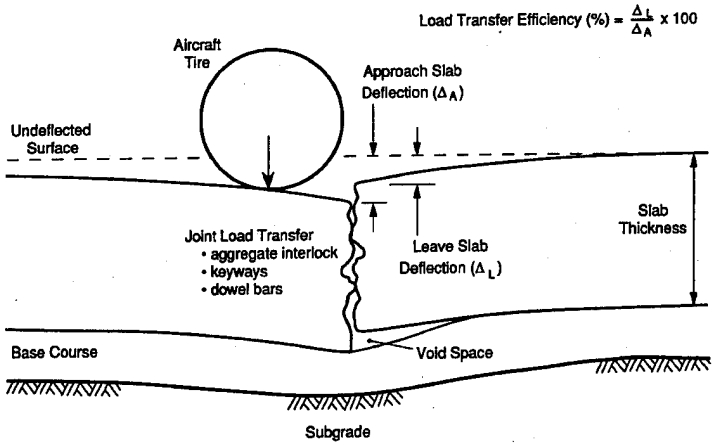

Figure 37. Load transfer efficiency across a joint.

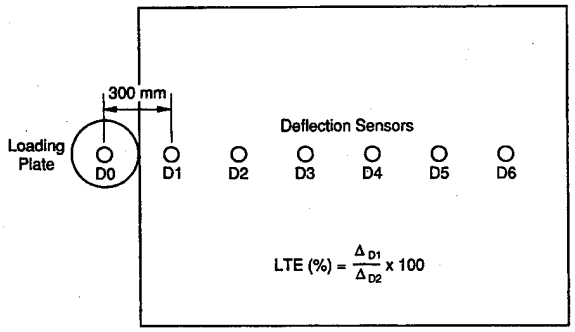

Figure 38. Placement of FWD sensors for load transfer efficiency test.

to determine the amount of deflection on either side of the joint as illustrated in Figure 37.

The Corps of Engineers' method (TM 5-826-5, U.S. Army, no date) for calculating the Joint Transfer Efficiency (JTE) using the deflections obtained with the FWD is

$$JTE = \frac{\delta_1}{\delta_0}$$

where JTE = joint transfer efficiency
δ_0 = center plate deflection
δ_1 = deflection measured across joint.

With the FWD, the center sensor was placed on one side of the joint and the second sensor, located 300 mm away from the center of the loading plate, was placed across the joint. This is illustrated in Figure 38. The JTE values across the transverse, longitudinal and corner joints, as calculated from the equation above for both CWA and OCA, are presented in Tables 11 and 12. The JTE values presented in the tables are the average from the four drop heights (joint and load transfer have been used interchangeably in the literature). In this report, a distinction is made between joint (JTE) and load transfer efficiency (LTE). Joint transfer efficiency as shown above is the ratio of the deflections on either side of the joint from an applied load. Load (or stress) transfer is the ratio of amount of stress that is transferred across the joint. For a perfect transfer, 50% of the stress is transferred across the joint.

From his study, Foxworthy (1985) reported the following:

1. JTE increased with increasing temperature and the relationship between JTE and temperature was the same whether he used air or pavement temperatures.
2. The type of joint construction affected the rate at which LTE changed with temperature.
3. The JTE was not affected by the FWD load used during the test.
4. The JTE was the same across transverse joints when measured from the approach or leave slab on airfield pavements (see Fig. 37). However, across longitudinal joints, the LTE values were higher when measured from the leave slab.

Foxworthy (1985) developed relationships for predicting the LTE. He found that, in general, an S type curve could be used to fit his results concerning load transfer efficiency and temperature (Fig. 39). The JTE–temperature relationships obtained by Foxworthy were from tests conducted at different times of the day where the only changes that were occurring were in the PCC layer. Since the base and subgrade strengths were changing very little with time, these results may not be applicable to pavements during thaw-weakening periods. So, we used the limited data collected at OCA and CWA to study the effects of changing subbase–subgrade stiffness during spring thaw on JTE.

Loads were transferred across transverse joints with dowels or aggregate interlocks and across longitudinal joints by the use of keyways, aggregate interlocks or tiebars. Typical changes at CWA are shown in Figures 40 and 41. We found two basic trends at CWA and only the first at OCA:

1. In general, the transverse JTE increased with increasing temperature, similar to that reported by Fox-

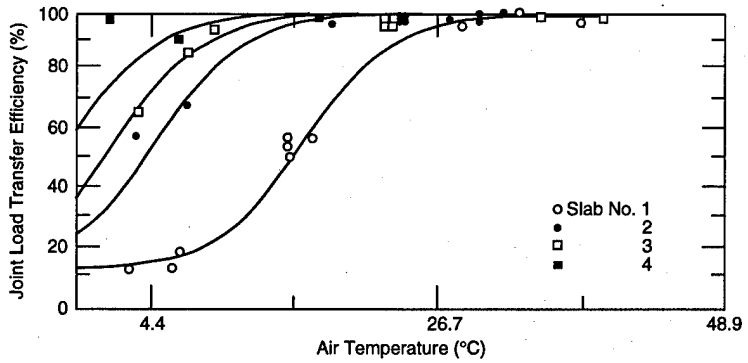

Figure 39. Relationship between air temperature and transverse joint transfer efficiency (after Foxworthy 1985).

Table 11. Joint transfer efficiencies at Central Wisconsin Airport (%).

a. Across transverse joints.

Date	1	2	3	4	5	6	7	8	9
20 Mar 86	59.0	51.9	81.6	86.4	55.0	49.7	59.0	60.7	42.5
24 Mar 86	63.4	32.2	89.4	85.4	69.9	64.0	63.2	86.5	67.0
27 Mar 86	68.8	49.8	94.5	95.2	47.6	60.8	75.0	86.7	58.1
4 Apr 86	77.1	78.4	92.0	92.5	47.1	60.7	74.4	85.1	78.0
7 Apr 86	77.6	82.1	93.2	94.7	49.3	90.1	71.7	90.4	92.3
10 Apr 86	71.9	71.6	92.9	89.5	59.1	61.3	80.4	77.0	74.1
14 Apr 86	75.0	76.6	92.3	94.5	67.8	65.4	84.4	91.8	82.8
17 Apr 86	71.3	72.6	91.7	94.0	59.8	90.5	71.2	71.9	91.7
21 Apr 86	74.3	75.2	89.2	89.5	71.1	82.4	83.7	84.3	91.1
24 Apr 86	70.9	91.8	90.3	91.6	70.4	92.6	80.9	80.2	92.9

Date	10	11	12	13	15	16	17	18	19
18 Mar 86	81.6	88.8	75.6	94.3	46.3	51.3	36.1	33.4	56.6
24 Mar 86	76.0	58.2	55.1	86.4	62.7	68.6	34.1	50.3	45.8
27 Mar 86	88.6	73.7	66.0	91.9	61.5	67.4	37.0	54.8	56.2
4 Apr 86	90.7	67.0	63.6	102.6	54.8	79.5	50.0	62.2	60.6
7 Apr 86	96.5	90.4	102.9	103.1	64.3	86.8	74.3	76.8	86.9
10 Apr 86	94.7	73.2	63.4	99.6	60.8	82.9	50.6	67.1	63.8
14 Apr 86	94.6	77.0	67.0	93.9	43.1	94.6	57.5	59.4	69.8
17 Apr 86	95.6	72.1	61.7	95.5	58.7	89.9	67.2	67.7	78.0
21 Apr 86	92.4	74.1	59.1	91.2	57.8	69.8	58.7	61.4	70.4
24 Apr 86	93.8	68.5	81.6	92.4	66.2	84.0	89.6	82.0	89.9

Date	20	21	22	23	24	25	26	27	28
18 Mar 86	77.1	86.0	75.5	80.0	51.5	65.2	70.6	77.6	35.9
24 Mar 86	62.6	—	—	—	—	—	—	—	78.7
27 Mar 86	81.3	76.8	85.8	90.9	53.9	68.7	66.0	85.8	59.5
4 Apr 86	79.6	80.9	80.3	87.3	57.6	65.6	65.6	94.5	73.5
7 Apr 86	89.5	87.7	88.9	87.0	59.4	68.9	72.7	92.0	32.8
10 Apr 86	80.7	77.3	80.7	84.6	57.4	67.7	70.4	91.7	72.8
14 Apr 86	84.5	89.6	78.0	88.7	69.2	75.0	74.2	94.3	25.9
17 Apr 86	85.8	81.3	77.5	89.7	57.2	63.4	64.2	93.0	30.4
21 Apr 86	80.7	80.2	72.0	82.8	59.7	68.6	64.7	89.4	26.6
24 Apr 86	92.7	84.3	91.5	83.2	58.3	71.8	67.4	92.7	29.4

b. Across longitudinal joints.

Date	1	2	3	4	5	6	7	8	9
20 Mar 86	47.5	56.8	40.7	42.7	14.2	31.6	40.5	36.7	24.0
24 Mar 86	28.6	74.5	35.7	85.1	32.9	74.4	31.5	25.2	27.0
4 Apr 86	15.8	23.7	46.1	82.8	6.9	78.1	82.1	7.4	12.2
7 Apr 86	19.0	20.1	52.4	92.9	7.5	47.2	71.6	31.1	27.3
17 Apr 86	14.9	18.8	23.5	88.1	14.6	57.7	59.1	11.0	40.8
21 Apr 86	11.4	23.7	50.0	—	13.5	77.2	64.8	6.8	21.3

Date	10	11	12	13	15	16	17	18	19
18 Mar 86	50.2	67.2	—	—	9.3	62.2	15.2	11.0	65.4
24 Mar 86	57.3	—	—	—	24.6	43.0	42.3	59.1	41.3
4 Apr 86	62.7	—	—	98.8	45.4	63.0	66.2	43.5	35.7
7 Apr 86	76.6	—	—	98.2	44.0	49.5	68.8	52.1	39.0
14 Apr 86	15.5	—	—	98.3	73.5	77.2	27.9	86.3	45.4
21 Apr 86	14.4	—	—	92.4	—	—	—	—	—

Date	20	21	22	23	24	25	26	27	28
18 Mar 86	60.8	49.1	90.0	22.5	61.3	87.1	54.5	—	—
27 Mar 86	42.0	109.3	68.3	33.4	58.7	87.2	72.6	—	—
4 Apr 86	67.2	52.1	79.3	25.0	26.0	91.7	79.6	—	—
7 Apr 86	78.1	49.2	80.5	—	43.2	88.9	79.6	—	—
14 Apr 86	53.2	71.8	83.4	21.5	33.9	98.5	88.6	—	—
21 Apr 86	—	—	—	18.5	30.6	90.9	80.6	—	—

c. Across corner joints.

Date	1	2	3	4	5	6	7	8	9
20 Mar 86	61.0	23.1	99.4	85.0	33.6	30.5	78.6	64.2	33.0
24 Mar 86	77.0	24.6	100.0	84.0	68.3	65.6	61.3	66.0	29.3
4 Apr 86	73.4	56.7	94.8	90.7	62.7	39.0	84.3	82.6	64.7
7 Apr 86	69.4	65.0	93.6	94.5	61.6	53.2	67.6	55.1	81.6
17 Apr 86	62.5	73.9	94.5	91.4	54.4	53.9	71.5	63.0	65.0
21 Apr 86	57.3	78.0	99.8	84.4	51.9	73.3	85.6	84.7	79.2

Date	10	11	12	13	15	16	17	18	19
18 Mar 86	66.5	69.7	—	116.3	79.8	60.6	44.5	64.9	64.3
24 Mar 86	73.5	—	—	—	61.1	49.8	51.2	46.4	46.5
27 Mar 86	0.0	—	—	—	—	—	—	—	—
4 Apr 86	95.3	—	—	79.3	84.3	69.7	41.9	52.5	71.4
7 Apr 86	91.6	—	—	77.4	86.2	59.1	45.2	56.2	79.5
14 Apr 86	94.2	—	—	—	72.0	72.9	71.0	63.1	76.9
21 Apr 86	90.2	—	—	—	—	—	—	—	—

Date	20	21	22	23	24	25	26	27	28
18 Mar 86	80.0	70.9	83.9	88.4	64.5	64.7	42.9	—	—
27 Mar 86	64.9	58.9	69.9	91.4	55.4	71.0	45.2	—	—
4 Apr 86	82.2	80.9	77.3	92.8	64.5	68.6	57.4	—	—
7 Apr 86	80.7	75.3	83.0	89.7	57.4	69.0	53.9	—	—
14 Apr 86	89.6	79.3	86.1	92.9	73.1	78.9	67.3	—	—
21 Apr 86	—	—	—	89.3	64.7	69.9	53.0	—	—

Table 12. Joint transfer efficiencies at OCA (%).

a. Across transverse joints.

Date	*1*	*2*	*3*	*4*	*5*	*6*	*7*	*8*	*9*	*10*	*11*
15 Mar 86	38.1	22.4	57.1	30.3	27.4	19.5	39.6	69.7	57.9	36.8	48.3
26 Mar 86	58.3	16.2	64.7	—	28.1	11.6	37.6	96.8	76.1	36.3	58.8
29 Mar 86	71.7	25.8	62.9	84.0	88.5	25.3	48.2	98.3	94.8	91.5	93.6
5 Apr 86	64.4	22.9	63.3	70.8	73.8	21.3	42.3	44.5	66.6	40.1	81.0
9 Apr 86	54.4	15.0	57.8	20.5	39.4	12.6	42.1	12.3	33.0	22.7	61.8
12 Apr 86	75.3	13.8	62.0	31.0	51.0	13.3	45.7	12.9	51.2	50.2	82.5
16 Apr 86	63.9	20.0	56.7	42.3	43.0	49.1	37.7	21.8	47.2	58.0	77.2
23 Apr 86	77.2	27.7	63.5	93.3	85.7	27.9	42.8	34.1	89.1	90.2	97.2
26 Apr 86	94.3	41.2	77.8	94.7	94.7	76.3	54.2	76.2	92.6	93.7	100.6

Date	*12*	*13*	*14*	*15*	*16*	*19*	*20*	*21*	*22*	*23*	*24*
15 Mar 86	41.4	24.1	42.2	7.1	65.8	77.2	54.4	51.0	30.5	52.3	34.0
26 Mar 86	66.5	21.3	65.6	18.8	80.7	92.2	59.1	55.3	40.2	61.0	50.0
29 Mar 86	87.6	69.4	90.7	29.6	92.3	94.8	87.1	62.0	67.9	92.4	75.5
5 Apr 86	74.6	37.0	48.6	14.0	78.9	91.4	65.4	54.6	76.6	30.2	75.5
9 Apr 86	77.4	19.7	28.5	16.9	76.3	90.9	61.2	54.2	52.6	76.5	33.4
12 Apr 86	82.2	18.9	36.9	—	78.6	92.2	63.6	54.1	55.7	15.7	116.2
16 Apr 86	75.6	36.6	41.4	29.4	63.3	89.4	66.9	56.8	50.4	28.3	21.0
23 Apr 86	91.3	20.4	35.3	18.0	76.8	91.2	73.7	56.9	49.7	18.0	15.0
26 Apr 86	92.8	67.6	94.0	89.7	89.9	—	—	—	58.2	45.8	81.7

b. Across longitudinal joints.

Date	*1*	*2*	*3*	*4*	*5*	*6*	*7*	*8*	*9*	*10*	*11*
15 Mar 86	24.9	61.2	67.7	34.8	17.7	20.1	80.7	45.9	50.6	11.0	27.4
29 Mar 86	16.6	73.5	86.1	83.3	17.0	27.5	98.9	72.3	87.5	15.8	46.4
5 Apr 86	15.8	80.1	89.0	59.6	18.7	19.6	92.8	77.8	74.7	23.3	17.9
12 Apr 86	11.7	82.1	83.1	89.8	17.2	14.5	99.5	84.0	49.1	17.2	18.3
26 Apr 86	80.1	106.4	86.3	88.1	25.0	49.4	92.9	84.3	91.6	39.5	82.5

Date	*12*	*13*	*14*	*15*	*16*	*19*	*20*	*21*	*22*	*23*	*24*
15 Mar 86	14.4	14.6	11.1	14.7	70.3	70.3	64.8	20.7	45.2	32.7	74.4
29 Mar 86	16.8	49.8	13.0	21.5	87.3	89.7	76.1	76.8	93.5	90.0	99.4
5 Apr 86	31.7	32.3	26.4	27.2	53.9	81.8	62.7	68.0	80.7	88.6	99.4
12 Apr 86	16.1	32.4	24.8	20.5	99.0	83.7	37.4	89.1	20.9	75.9	89.6
26 Apr 86	28.1	35.0	27.3	64.0	81.8	—	—	—	52.4	93.4	97.8

c. Across corner joints.

Date	*1*	*2*	*3*	*4*	*5*	*6*	*7*	*8*	*9*	*10*	*11*
15 Mar 86	33.6	27.2	50.7	84.9	17.5	16.6	41.3	29.3	13.8	15.6	20.9
29 Mar 86	52.7	76.3	53.1	90.5	32.3	13.4	63.7	87.4	42.5	75.6	52.6
5 Apr 86	56.0	41.8	59.2	85.5	25.3	10.2	57.4	66.1	31.0	32.6	103.6
12 Apr 86	47.5	26.3	49.3	36.0	13.7	6.6	42.0	17.7	47.4	33.4	40.6
26 Apr 86	46.9	95.8	66.7	92.4	55.3	—	68.2	91.7	90.1	85.4	70.1

Date	*12*	*13*	*14*	*15*	*16*	*19*	*20*	*21*	*22*	*23*	*24*
15 Mar 86	27.4	5.2	87.0	4.4	52.7	84.6	31.1	27.5	22.4	13.2	29.3
29 Mar 86	73.5	85.1	93.7	11.9	72.8	90.0	71.7	29.9	61.1	21.3	69.2
5 Apr 86	66.3	17.8	69.8	4.2	79.2	94.6	65.5	113.1	23.2	41.7	69.2
12 Apr 86	82.1	29.7	47.4	5.1	87.2	96.5	66.9	53.3	80.5	22.4	18.2
26 Apr 86	90.4	78.4	96.7	31.4	84.4	—	—	—	90.0	91.9	72.0

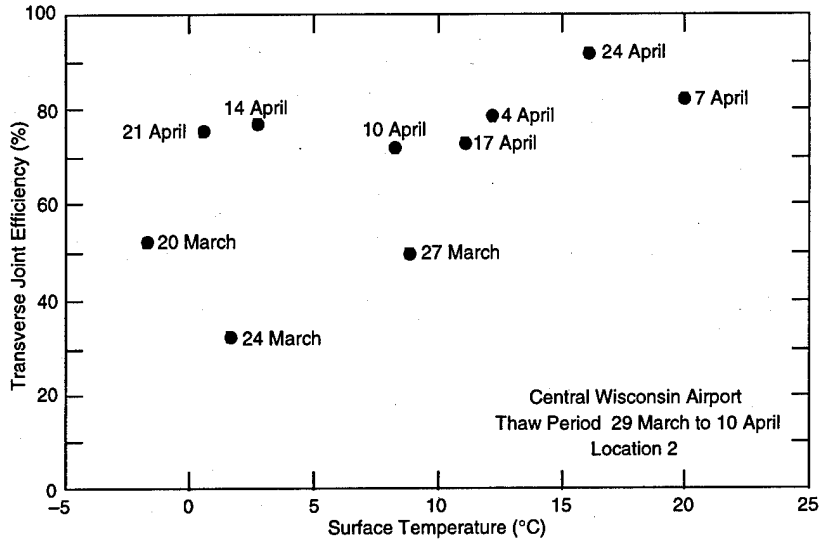

a. FWD location 2.

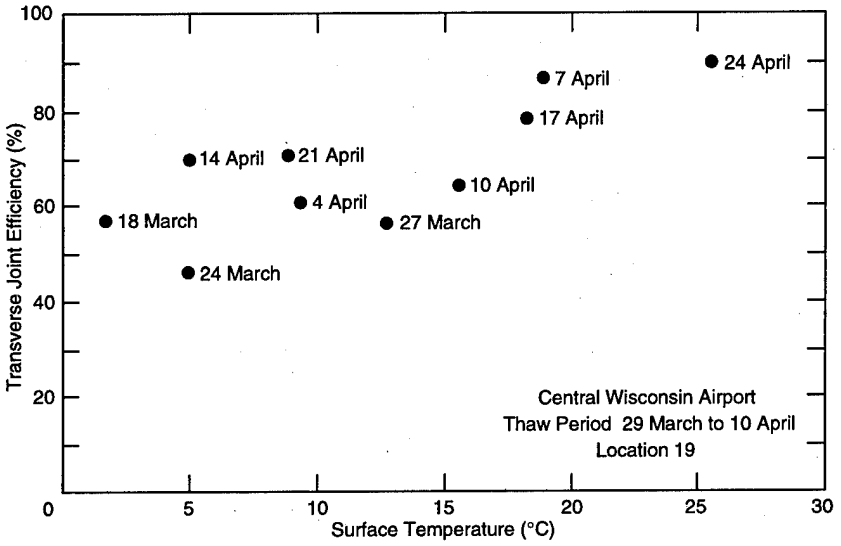

b. FWD location 19.

Figure 40. Change of transverse joint efficiency with surface temperature.

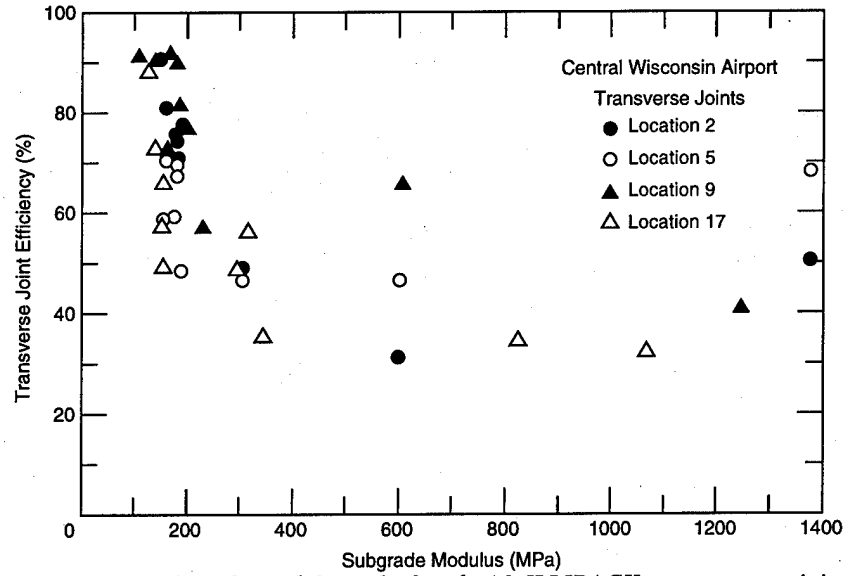

Figure 41. Effect of subgrade modulus calculated with ILLIBACK on transverse joint efficiency.

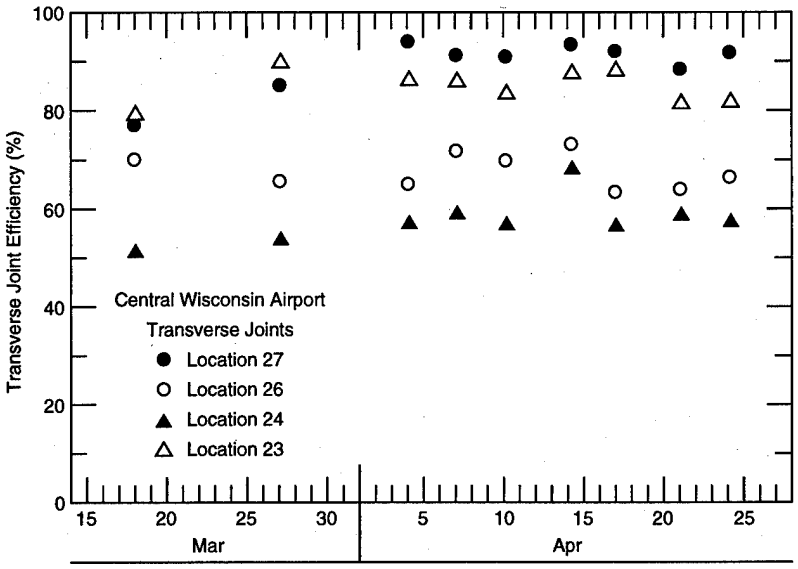

Figure 42. Change in transverse joint transfer with time on taxiway B.

worthy (1985) (Fig. 40). In addition, we determined that increases in temperature did not cause increases in JTE during the early thaw period; the JTE in most cases decreased. As thaw progressed, the JTE recovered. In the late thaw period, the JTE was basically a linear function of temperature (Fig. 40b). The most significant effect of thawing was related to the base–subgrade modulus (Fig. 41).

2. At the CWA FWD locations where the base course was 1.2 m thick, the effect of temperature on the transverse joint efficiency was negligible (Fig. 42). It should also be noted that the thickness of the PCC layer is 330 mm compared to the other sites, where it ranged from 254 to 305 mm. This increase in thickness may also contribute to the negligible effect of surface temperature on the JTE. This was not observed at OCA.

3. With a few exceptions, as shown in Tables 11b and 12b, the JTE was low across the longitudinal joints at CWA and OCA. The data infer that, in general, the longitudinal joints were weak with respect to load transfer.

The LTE was determined for the transverse joints both at CWA and OCA using the procedure outlined in Hammons and Pittman (1993). The LTE across a joint is estimated as a function of the radius of relative stiffness (l) and the JTE. The JTE is determined from FWD deflection data as discussed above. The radius of relative stiffness (l) is determined from the normalized basin area (*AREA*) from a unique relationship developed by Ioannides (1989). This relationship for a dense liquid foundation is reproduced in Figure 43. A sixth-order polynomial equation was developed for

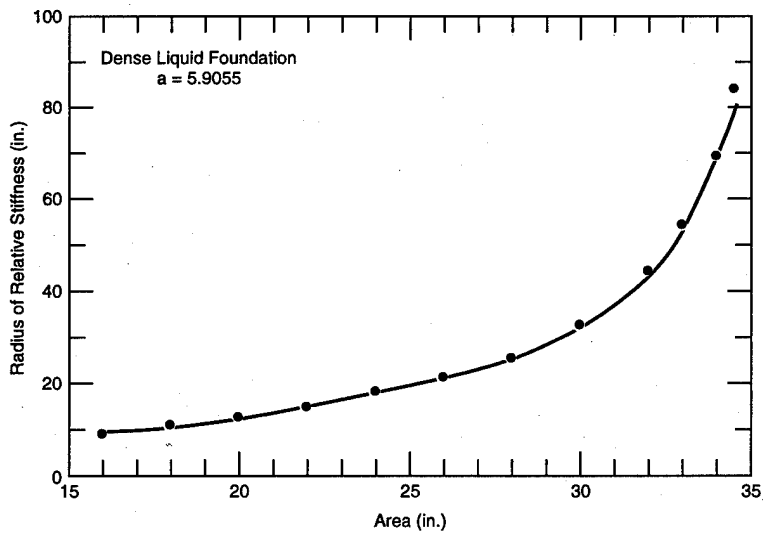

Figure 43. Relationship between AREA *and* l *for a dense liquid foundation,* a = *5.90655 in. (after Hammon and Pittman 1993).*

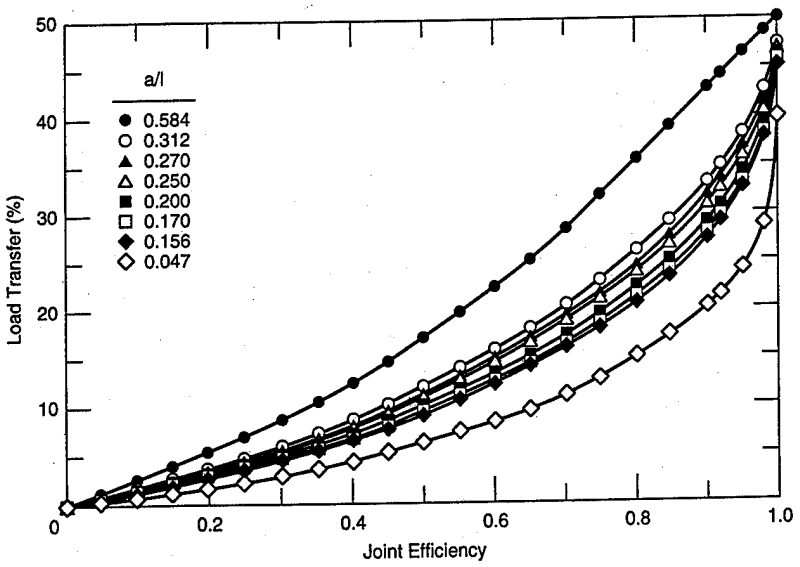

Figure 44. Interpolated relationships between joint efficiency and load transfer as a function of a/l *(after Hammon and Pittman 1993).*

this relationship and is in the form of

$$l = 0.5 - (1.24AREA) + 1.21AREA^2 - 0.1803AREA^3$$

$$+ 0.011098AREA^4 - 0.0003075AREA^5$$

$$+ 0.000003198AREA^6$$

and

$$AREA = 6\left[1 + 2\left(\frac{\delta_1}{\delta_0}\right) + 2\left(\frac{\delta_2}{\delta_0}\right) + \left(\frac{\delta_3}{\delta_0}\right)\right]$$

where l = radius of relative stiffness (inches)
δ_i= FWD deflections (inches)
$AREA$ = normalized deflection basin area
i = deflection sensor number.

With the ratio of radius of the FWD loading plate (a) to the radius of relative stiffness (a/l) and the joint efficiency, Figure 44 was used to calculate the load transfer efficiency. Figure 44 was developed by Tabatabaie et al. (1979) and modified by Hammons and Pittman (1993). The results of the load transfer across transverse joints were determined at both CWA and OCA and are presented in Figure 45. We found that the relationship below can be used to estimate the LTE of transverse joints using FWD JTE data.

$$LTE\ (\%) = 1.912e^{3.115(JTE)}$$

where JTE is joint transfer efficiency (decimal).

We did not attempt to develop similar relationships for the longitudinal joint because of the low JTE values

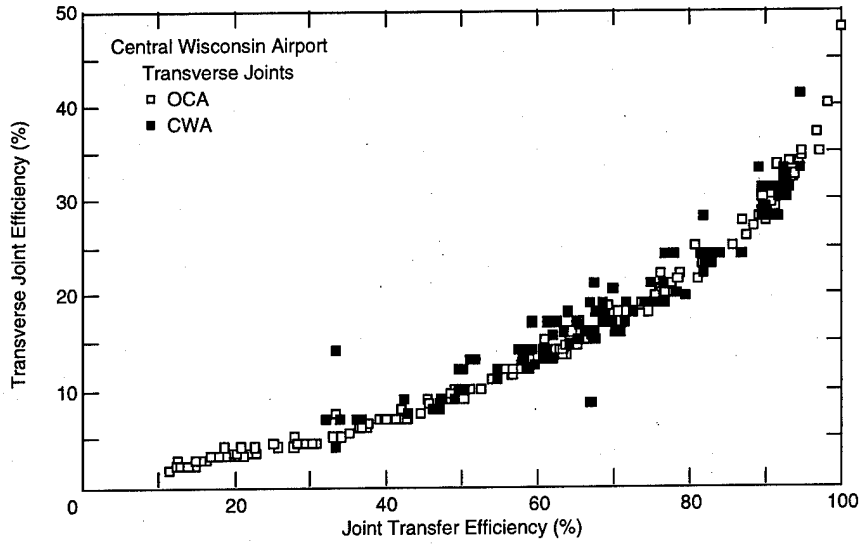

Figure 45. Relationship between JTE and LTE for transverse joints.

and also because of the small database. However, because of the unique relationship between JTE and LTE shown in Figure 45, it may be possible to apply the same relationship to longitudinal joints.

To meet the criterion that the LTE of the joint be not less than 25%, the JTE should exceed 80%. If this is the case, a review of Tables 11a and 12a indicates that many of the joints at CWA and OCA were below capacity during the thawing period. At the end of thaw, nearly all of them met the 25% criterion. The results indicate that most of the damage to transverse joints probably occurs during the winter and spring thawing period.

PROPOSED PAVEMENT EVALUATION PROCEDURE

A methodology is proposed for evaluating pavement performance during the thaw-weakening periods using FWD deflection data. From this study, we found that, for PCC pavement, the composite subgrade modulus (base and subgrade) can be estimated from the deflection basin area and Figure 46 or from the following equation

$$E_{sub} = 154{,}319\Delta^{-1.1708}$$

where E_{sub} is the subgrade modulus (MPa), and Δ is deflection basin area (mm^2). The horizontal tensile stress at the bottom of the PCC layer was found to be a function of pavement thickness and E_{sub} or the coefficient of subgrade reaction (k) from the following equations for either a Boeing 757 or for a MD-DC9.

$$\sigma_{tensile} = 7360 - 1.5E_{sub} - 17t$$

$$\sigma_{tensile} = 7389 - 3.02k - 17.5t$$

or, with respect to total basin area, an estimate could be made using

$$\sigma_{tensile} = 7.35A_T$$

where $\sigma_{tensile}$ = horizontal tensile stress at the bottom of the PCC layer (kPa)
k = coefficient of subgrade reaction (MN/m^3)
t = PCC layer thickness (mm).

The LTE across transverse joints can be estimated from the JTE from Figure 47 or from the following equation

$$LTE\ (\%) = 1.912e^{3.115(JTE)}$$

where JTE is the joint transfer efficiency (decimal)

$$JTE = \frac{\delta_u}{\delta_i}$$

and δ_u is FWD deflection on an unloaded slab and δ_i is FWD deflection on a loaded slab.

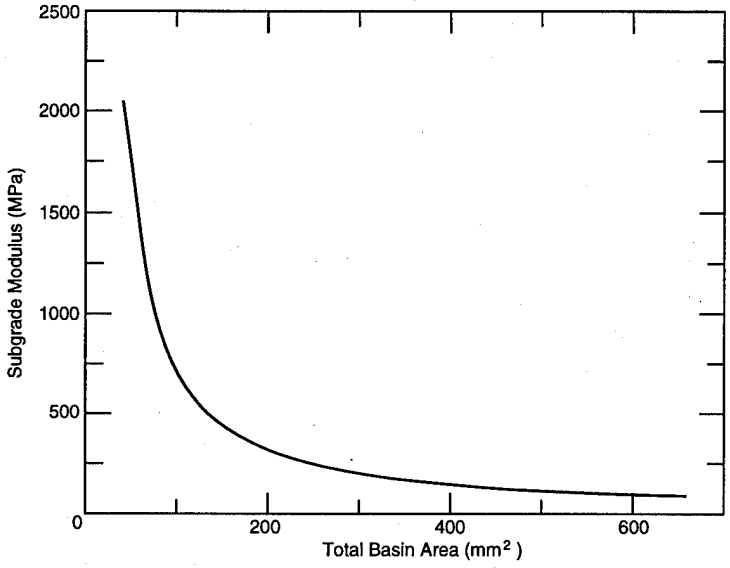

Figure 46. Relationship between total basin area and subgrade modulus.

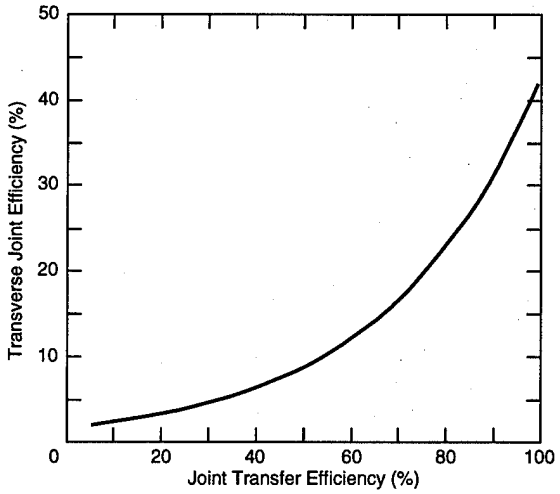

Figure 47. Relationship between JTE and LTE.

CONCLUSIONS

During the spring thawing period, the JTE was a function not only of the surface temperature but also of subgrade stiffness. Near the end of thaw, the JTE was basically solely a function of the surface temperature.

Unique relationships were developed between FWD deflections and the subgrade modulus (E_{sub}) and between the FWD deflections and the coefficient of subgrade coefficient (k). Additional relationships were developed between the PCC layer thickness and either E_{sub} or k and the horizontal tensile stress ($\sigma_{tensile}$) at the bottom of the PCC layer.

A relationship was also developed for determining the load transfer across transverse joints on the basis of JTE calculated from FWD deflection data. This relationship could be also used for longitudinal joints.

The developed relationships allowed us to propose a methodology for evaluating PCC pavement performance during winter and thaw-weakening periods. However, this methodology could be used at other times of the year.

The relationships developed from this study should be verified at other sites. In particular, although there are only small differences in the horizontal stress relationships for the Boeing 757 and the MD-DC9, additional horizontal stress relationships may be needed for other aircraft.

Field measurements of horizontal stress or strain are necessary to verify these relationships.

LITERATURE CITED

Barenberg, E.J. and A.M. Ioannides (1989) Structural evaluation of concrete slabs using falling weight deflectometer results, Urbana-Champaign: Advanced Construction Technology Center, University of Illinois.

U.S. Army (no date) Nondestructive procedures for airfield pavement evaluation. Draft Technical Manual TM 5-826-5.

CMT, Inc. (1984) Pavement evaluation program—Central Wisconsin Airport.

ERES Consultants (1985) Structural evaluation of runway 3-21.

Foxworthy, P.T. (1985) Concepts for the Development of a Nondestructive Testing and Evaluation System for Rigid Airfield Pavements. Ph.D. Dissertation, University of Illinois at Urbana-Champaign (unpublished).

Hammons M.I. and D.W. Pittman (1993) Effectiveness of load transfer devices. Draft Final Report. USA Waterways Experiment Station, Vicksburg, Mississippi.

Ioannides, A.M., E.J. Barenberg and J.A. Lary (1989) Interpretation of falling weight deflectometer results using principles of dimensionless analysis. Advanced Construction Technology Center, Document No. 89-51-01.

Irwin L.H., W.S. Yang and R.N. Stubstad (1989) Deflection reading accuracy and layer thickness accuracy in backcalculation of pavement layer moduli. In *Proceedings, Nondestructive Testing of Pavement and Backcalculation of Moduli* (A.J. Bush III and G.Y. Baladi, Ed.). ASTM STP 1026, p. 171–188.

Janoo, V.C. and R.L. Berg (1990) Predicting pavement response during thaw weakening periods using the falling weight deflectometer. In *Proceedings, Third International Conference on Bearing Capacity of Roads and Airfields, Trondheim, Norway,* vol. 1, p. 31–40.

Janoo, V.C. and R.L. Berg (1991) Asphalt concrete airfield pavement evaluation during thaw weakening periods using the falling weight deflectometer. USA Cold Regions Research and Engineering Laboratory, CRREL Report 91-7.

Janoo, V.C. and R.L. Berg (1996) PCC airfield pavement response to thaw weakening periods: Data. USA Cold Regions Research and Engineering Laboratory, Internal Report 1155.

Mead and Hunt, Inc. (1988) Runway 11/29 strengthening design study.

Stark, J. and R.L. Berg (1989) Performance of pavement at Central Wisconsin Airport. In *Proceedings, 5th International Conference on Cold Regions Engineering*. New York: American Society of Civil Engineers.

REPORT DOCUMENTATION PAGE

Form Approved
OMB No. 0704-0188

1. AGENCY USE ONLY (Leave blank)	2. REPORT DATE	3. REPORT TYPE AND DATES COVERED
	May 1996	

4. TITLE AND SUBTITLE

PCC Airfield Pavement Response During Thaw-Weakening Periods: A Field Study

5. FUNDING NUMBERS

PR: 4A762784AT42
MA: BS
WU: BS/036

6. AUTHORS

Vincent C. Janoo and Richard L. Berg

7. PERFORMING ORGANIZATION NAME(S) AND ADDRESS(ES)

U.S. Army Cold Regions Research and Engineering Laboratory
72 Lyme Road
Hanover, New Hampshire 03755-1290

8. PERFORMING ORGANIZATION REPORT NUMBER

Special Report 96-12

9. SPONSORING/MONITORING AGENCY NAME(S) AND ADDRESS(ES)

Federal Aviation Administration
Technical Center
Atlantic City International Airport
New Jersey 08405

and

Office of the Chief of Engineers
Washington, D.C. 20314-1000

10. SPONSORING/MONITORING AGENCY REPORT NUMBER

11. SUPPLEMENTARY NOTES

12a. DISTRIBUTION/AVAILABILITY STATEMENT

Approved for public release; distribution is unlimited.

Available from NTIS, Springfield, Virginia 22161.

12b. DISTRIBUTION CODE

13. ABSTRACT (*Maximum 200 words*)

This investigation is part of CRREL's on-going characterization of pavement performance in seasonal frost areas. As part of the research, CRREL conducted several field studies for the Federal Aviation Administration (FAA) on the response of airport pavements during thaw-weakening periods at three civil airports in Wisconsin where the design freezing index in the area was around 900 to 1100°C-days and frost penetration ranged between 1250 and 2000 mm. This study focused on the performance of Portland Cement Concrete (PCC) pavements during the spring thaw-weakening period. The sites were instrumented with subsurface thermocouples and Falling Weight Deflectometer (FWD) tests were conducted during the spring thaw period at the center of the slab and across the joints. An analysis of the FWD data and backcalculation of the layer moduli using ILLIBACK and WESDEF was conducted. Unique relationships between the FWD deflections and the subgrade modulus and coefficient of subgrade reaction were obtained. Additional relationships were developed using the FWD deflections, PCC thickness and the horizontal tensile stress at the bottom of the PCC layer. A relationship between load transfer across joints and FWD deflections was also developed. On the basis of the relationships obtained in this study, a methodology for evaluating PCC pavements during spring thaw was developed. However, this methodology needs to be verified for other subgrade types and areas with other design freezing indices.

14. SUBJECT TERMS

Evaluation, Pavement, Thaw-weakening, Load transfer, PCC pavements

15. NUMBER OF PAGES

44

16. PRICE CODE

17. SECURITY CLASSIFICATION OF REPORT	18. SECURITY CLASSIFICATION OF THIS PAGE	19. SECURITY CLASSIFICATION OF ABSTRACT	20. LIMITATION OF ABSTRACT
UNCLASSIFIED	UNCLASSIFIED	UNCLASSIFIED	UL